

SYRTHES 5.0  
Validation Manual

I. Rupp, C. Peniguel

2022

## AVERTISSEMENT / CAUTION

L'accès à ce document, ainsi que son utilisation, sont strictement limités aux personnes expressément habilitées par EDF.

EDF ne pourra être tenu responsable, au titre d'une action en responsabilité contractuelle, en responsabilité délictuelle ou de tout autre action, de tout dommage direct ou indirect, ou de quelque nature qu'il soit, ou de tout préjudice, notamment, de nature financier ou commercial, résultant de l'utilisation d'une quelconque information contenue dans ce document.

Les données et informations contenues dans ce document sont fournies "en l'état" sans aucune garantie expresse ou tacite de quelque nature que ce soit.

Toute modification, reproduction, extraction d'éléments, réutilisation de tout ou partie de ce document sans autorisation préalable écrite d'EDF ainsi que toute diffusion externe à EDF du présent document ou des informations qu'il contient est strictement interdite sous peine de sanctions.

---

The access to this document and its use are strictly limited to the persons expressly authorized to do so by EDF.

EDF shall not be deemed liable as a consequence of any action, for any direct or indirect damage, including, among others, commercial or financial loss arising from the use of any information contained in this document.

This document and the information contained therein are provided "as are" without any warranty of any kind, either expressed or implied.

Any total or partial modification, reproduction, new use, distribution or extraction of elements of this document or its content, without the express and prior written consent of EDF is strictly forbidden. Failure to comply to the above provisions will expose to sanctions.

# Summary

	AVERTISSEMENT / CAUTION . . . . .	1
<b>1</b>	<b>Introduction</b>	<b>6</b>
<b>I</b>	<b>CONDUCTION</b>	<b>8</b>
<b>2</b>	<b>Introduction</b>	<b>9</b>
<b>3</b>	<b>RECTAN</b>	<b>10</b>
3.1	Test case description . . . . .	10
3.1.1	Geometry . . . . .	10
3.1.2	Physical conditions . . . . .	10
3.1.3	Initial conditions, boundary conditions . . . . .	11
3.2	Analytical solution . . . . .	11
3.3	Calculation description . . . . .	11
3.3.1	Meshes . . . . .	11
3.4	Presentation of results . . . . .	12
3.4.1	Temperature field . . . . .	12
3.4.2	Comparison calculation results / analytical values . . . . .	12
3.5	Synthesis . . . . .	15
<b>4</b>	<b>SQUARE-H</b>	<b>16</b>
4.1	Test case description . . . . .	16
4.1.1	Geometry . . . . .	16
4.1.2	Physical conditions . . . . .	16
4.1.3	Initial conditions, boundary conditions . . . . .	17
4.2	Analytical solution . . . . .	17
4.3	Calculations description . . . . .	17
4.3.1	Mesh . . . . .	17
4.4	Presentation of results . . . . .	18
4.4.1	Thermal fields at convergence . . . . .	18
4.4.2	Comparison calculation results / analytical value . . . . .	18
4.5	Synthesis . . . . .	19
<b>5</b>	<b>RING</b>	<b>20</b>
5.1	Test case description . . . . .	20
5.1.1	Geometry . . . . .	20
5.1.2	Physical conditions . . . . .	20
5.1.3	Initial conditions, boundary conditions . . . . .	21
5.2	Analytical solution . . . . .	21
5.3	Calculations description . . . . .	21
5.3.1	Mesh . . . . .	21
5.4	Presentation of results . . . . .	21

5.4.1	Thermal fields inside the ring . . . . .	21
5.4.2	Comparison calculation results / analytical value . . . . .	23
5.5	Synthesis . . . . .	24
<b>6</b>	<b>RING-H</b>	<b>26</b>
6.1	Test case description . . . . .	26
6.1.1	Geometry . . . . .	26
6.1.2	Physical conditions . . . . .	26
6.1.3	Initial conditions, boundary conditions . . . . .	27
6.2	Analytical solution . . . . .	27
6.3	Calculations description . . . . .	27
6.3.1	Mesh . . . . .	27
6.4	Presentation of results . . . . .	28
6.4.1	Thermal fields inside the ring . . . . .	28
6.4.2	Comparison calculation results / analytical value . . . . .	28
6.5	Synthesis . . . . .	31
<b>7</b>	<b>SPHERE</b>	<b>32</b>
7.1	Test case description . . . . .	32
7.1.1	Geometry . . . . .	32
7.1.2	Physical conditions . . . . .	32
7.1.3	Initial conditions, boundary conditions . . . . .	33
7.2	Analytical solution . . . . .	33
7.3	Calculation description . . . . .	33
7.3.1	Mesh . . . . .	33
7.4	Presentation of results . . . . .	34
7.4.1	Temperature field inside the sphere . . . . .	34
7.4.2	Comparison calculation results / analytical values . . . . .	34
7.5	Synthesis . . . . .	36
<b>8</b>	<b>BRICK</b>	<b>37</b>
8.1	Test case description . . . . .	37
8.1.1	Geometry . . . . .	37
8.1.2	Physical conditions . . . . .	37
8.1.3	Initial conditions, boundary conditions . . . . .	37
8.2	Analytical solution . . . . .	38
8.3	Calculations description . . . . .	38
8.3.1	Mesh . . . . .	38
8.4	Presentation of results . . . . .	38
8.4.1	Thermal field inside the brick . . . . .	38
8.4.2	Comparison calculated results / analytical value . . . . .	38
8.5	Synthesis . . . . .	41
<b>II</b>	<b>RADIATION</b>	<b>42</b>
<b>9</b>	<b>Introduction</b>	<b>43</b>
<b>10</b>	<b>View factors</b>	<b>44</b>
10.1	View factors in dimension 3 . . . . .	44
10.1.1	View factor between 2 face to face rectangular faces . . . . .	45
10.1.2	Case of 2 facets making an angle . . . . .	46
10.1.3	View factors in a cylinder . . . . .	48
10.2	Axisymmetric view factors . . . . .	49
10.2.1	Case of 2 rings on a cylinder . . . . .	49

10.2.2	Case of 2 rings on a cone . . . . .	50
10.2.3	Case of a ring on a cone, the other on a cylinder . . . . .	51
10.2.4	Case of 2 rings face to face . . . . .	52
10.2.5	Hidden faces : disk perpendicular to a cylinder . . . . .	53
10.2.6	Hidden faces : two concentric cylinders . . . . .	55
10.2.7	Hidden faces : cone and disk . . . . .	57
10.3	Summary of view factor validation . . . . .	58
<b>11</b>	<b>Solver validation</b>	<b>59</b>
<b>12</b>	<b>CHANNEL_RAD</b>	<b>62</b>
12.1	Test case description . . . . .	62
12.1.1	Geometry . . . . .	62
12.1.2	Physical conditions . . . . .	62
12.1.3	Initial conditions, boundary conditions . . . . .	62
12.2	Analytical solution . . . . .	63
12.3	Calculation description . . . . .	63
12.3.1	Meshes . . . . .	63
12.4	Presentation of results . . . . .	63
12.4.1	Comparison calculation results / analytical value . . . . .	64
12.4.2	Thermal field inside plates . . . . .	64
12.4.3	Study of calculation's convergence . . . . .	66
12.5	Synthesis . . . . .	66
<b>13</b>	<b>CYLINDERS_2D_RAD</b>	<b>67</b>
13.1	Test case description . . . . .	67
13.1.1	Geometry . . . . .	67
13.1.2	Physical conditions . . . . .	67
13.1.3	Initial conditions, boundary conditions . . . . .	68
13.2	Analytical solution . . . . .	68
13.3	Calculation description . . . . .	70
13.3.1	Meshes . . . . .	70
13.4	Presentation of results . . . . .	71
13.4.1	Temperature field inside cylinders . . . . .	71
13.4.2	Comparison calculation results / analytical values . . . . .	72
13.4.3	Study of calculation's convergence . . . . .	73
13.5	Synthesis . . . . .	73
<b>14</b>	<b>SPHERE_RAD</b>	<b>74</b>
14.1	Test case description . . . . .	74
14.1.1	Geometry . . . . .	74
14.1.2	Physical conditions . . . . .	74
14.1.3	Initial conditions, boundary conditions . . . . .	75
14.2	Analytical solution . . . . .	75
14.3	Calculation description . . . . .	77
14.3.1	Meshes . . . . .	77
14.4	Presentation of results . . . . .	78
14.4.1	Temperature field inside the spheres . . . . .	78
14.4.2	Comparison calculation results / analytical values . . . . .	79
14.4.3	Study of calculation's convergence . . . . .	80
14.5	Synthesis . . . . .	80

<b>15</b>	<b>CYLINDERS_3D_RAY</b>	<b>81</b>
15.1	Test case description . . . . .	81
15.1.1	Geometry . . . . .	81
15.1.2	Physical conditions . . . . .	81
15.1.3	Initial conditions, boundary conditions . . . . .	82
15.2	Analytical solution . . . . .	82
15.3	Calculation description . . . . .	83
15.3.1	Meshes . . . . .	83
15.4	Presentation of results . . . . .	84
15.4.1	Temperature inside cylinders . . . . .	84
15.4.2	Comparison calculation results / analytical values . . . . .	85
15.4.3	Study of calculation's convergence . . . . .	85
15.5	Synthesis . . . . .	86
<b>III</b>	<b>HEAT AND MASS TRANSFERS</b>	<b>87</b>
<b>16</b>	<b>WOODPANEL</b>	<b>88</b>
16.1	Test case description . . . . .	88
16.1.1	Geometry . . . . .	88
16.1.2	Physical conditions . . . . .	88
16.1.3	Boundary conditions . . . . .	89
16.2	Calculation description . . . . .	89
16.2.1	Meshes . . . . .	89
16.3	Presentation of results . . . . .	89

# Chapter 1

## Introduction

SYRTHES (SYstème de Résolution THERmique Solide) is a general purpose thermal code which allows to study very diverse industrial configurations.

Its goals are to solve thermal problems where conduction and radiation from wall to wall play a part.

Several documents have been written or can be downloaded from the website ([www.edf.fr/recherche/code-syrthes](http://www.edf.fr/recherche/code-syrthes)), and they allow to better understand SYRTHES possibilities:

- a user manual (including examples),
- some tutorials
- scientific publications presenting numerous industrial cases, especially in the nuclear field, in applications of electricity and more generally in configurations where thermal aspects are important ([7],[9],[8], [10],[11],[12],[2], [6],[1],[3]).

Since SYRTHES is used in numerous industrial studies, authors have put much effort on the validations aspects.

That step is important also because SYRTHES can be a part of coupled calculations where neutronic code (TRIPOLI), CFD codes (in particular *Code\_Saturne* or *neptune*) or mechanical code (*Code\_Aster*).

The work associated with the validation of SYRTHES has been voluntarily split in two phases.

- A first phase allows to check that on very elementary configurations, the approach retained and the numerical methods used (modelling, numerical methods, coding) give rigorous results. One wants to compare solutions only to reference solutions.
- A second phase consists in the elaboration of a validation base to check that the code is functioning correctly on more complex configurations. For conduction, reference [13] has been mainly used. For radiation reference [14] has been particularly used.

This document is divided in two distinct parts, the first one is devoted to the conduction solver while the second one focuses on the radiation and the coupling of conduction and radiation.

Among the fonctionnalités tested :

- permanent states en 2D (cartesian and axy) and 3D,
- boundary conditions (Dirichlet, flux, exchange,...)
- influence of the meshes sizes on results,
- transient and permanent configurations (axisymmetric and 3D),

- for the radiation, geometrical quantities (view factors) in numerous elementary situations.
- stationary configurations with a coupling between radiation and conduction

Part I

CONDUCTION

## Chapter 2

# Introduction

In this first part, one tests if the numerical approach and the algorithms used to solve the conduction within solids are valid. The different aspects tested are :

- reading of meshes,
- calculation of elementary matrices,
- taking into account the different boundary conditions (Dirichlet, flux,...)
- the solver,
- the writing of solids.

This first part is completely independent of the radiative aspects because quite a lot of industrial applications are only concerned with conductive aspects. Since the methodology used within the code numerically decouples these two aspects, it seems appropriate to test them independently.

Test cases allow to test :

- the 2D cartesian discretization,
- the 2D axisymmetrical discretization,
- the 3D discretization,
- the Dirichlet discretization,
- the exchange boundary condition,
- the influence of the meshes size,
- the influence of the time step used.

Obtaining analytical solutions may turn out to be quite difficult when configurations become more complex. In particular, we underline that no solutions have been found when material are anisotropic or when physical characteristics (density, heat capacity and conductivity) are temperature dependent. Setting such complex case using SYRTHES would be straightforward, but analytical solutions to be compared with are lacking. One underlines that the numerical methods used as well as the informatic paths are identical if physical properties are constant or temperature dependent.

All analytical solutions for transient and non linear are welcome. Such cases would then be tested and added to the present document.

## Chapter 3

# RECTAN

**Characteristics :** 2D, steady state, boundary conditions = imposed temperature

**Objectives :** Validation of thermal resolution inside a solid in 2D for a steady state. Validation of the treatment of Dirichlet's conditions.

### 3.1 Test case description

#### 3.1.1 Geometry

Consider a rectangle with the following dimensions :  $0 < x < 1 \text{ m}$ ,  $0 < y < 2 \text{ m}$ .

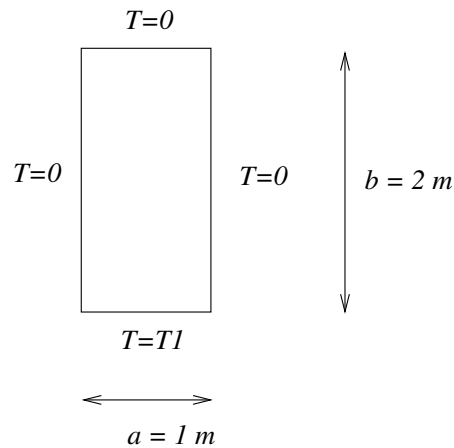


Figure 3.1: Solid domain

#### 3.1.2 Physical conditions

The solid is related to steel having following physical characteristics :

- conductivity  $k = 25 \text{ W/mK}$
- density  $\rho = 7700 \text{ kg/m}^3$
- specific heat  $C_p = 460 \text{ J/kgK}$

### 3.1.3 Initial conditions, boundary conditions

Initially (at  $t = 0$ ), the solid is at  $20^\circ C$ .

We impose on the lower side ( $y = 0$ ) a temperature  $T_1 = 1^\circ C$  and on the three other sides a temperature equal to  $0^\circ C$ .

## 3.2 Analytical solution

In the case of a plate of size  $0 < x < a$  and  $0 < y < b$  subject to following conditions : temperature  $T_1$  en  $y = 0$  and null temperature on the 3 other sides, the temperature in a point  $(x, y)$  of the plate is given by :

$$T(x, y) = \frac{4T_1}{\pi} \sum_{n=0}^{\infty} \frac{1}{2n+1} \sin\left(\frac{(2n+1)\pi x}{a}\right) \sinh\left(\frac{(b-y)(2n+1)\pi}{a}\right) \operatorname{cosech}\left(\frac{(2n+1)\pi b}{a}\right)$$

## 3.3 Calculation description

### 3.3.1 Meshes

The mesh has :

- 3081 nodes with 800 vertex nodes,
- 1482 triangles.

Border nodes  $y = 0$  have reference 1, those of other sides reference 2, others reference 0.

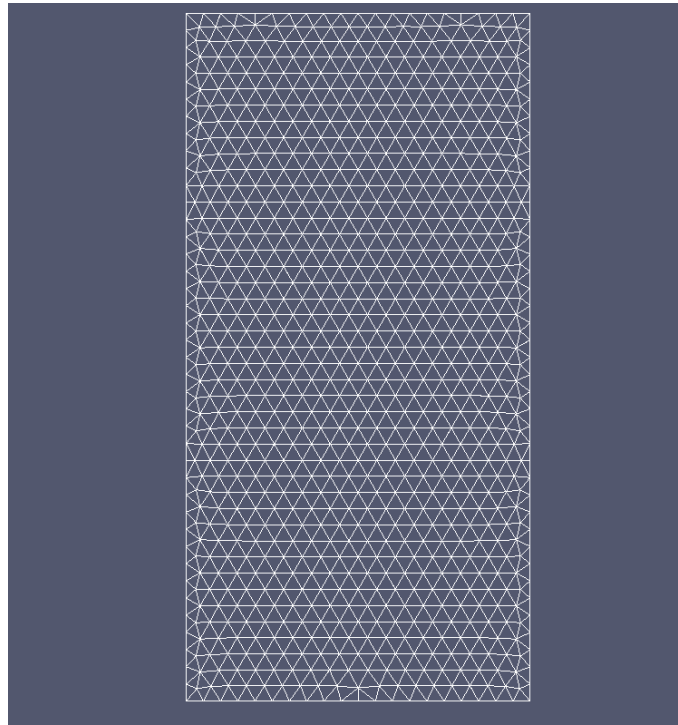


Figure 3.2: Mesh

### 3.4 Presentation of results

Steady state is reached after about 1.5 days.

For numerical simulation, we have used a time step equal to 500 seconds and convergence is reached after about 250 time steps.

#### 3.4.1 Temperature field

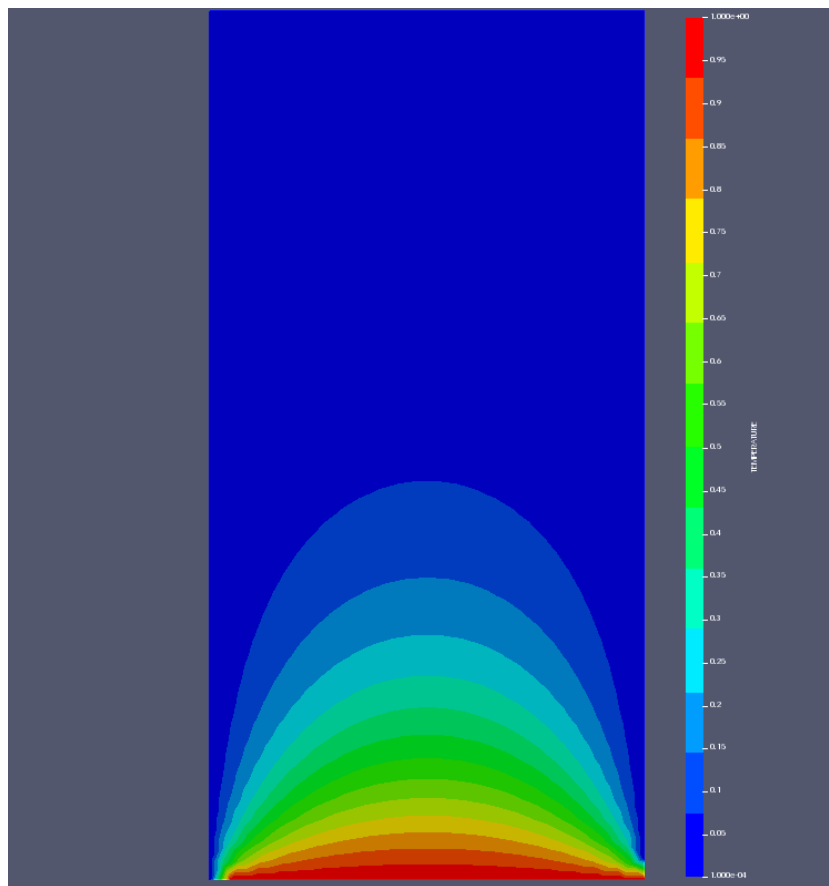


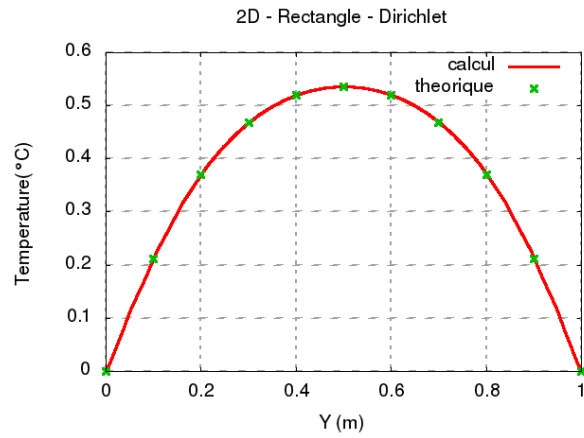
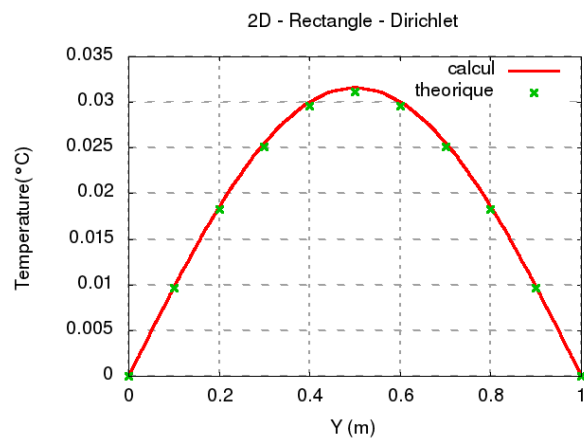
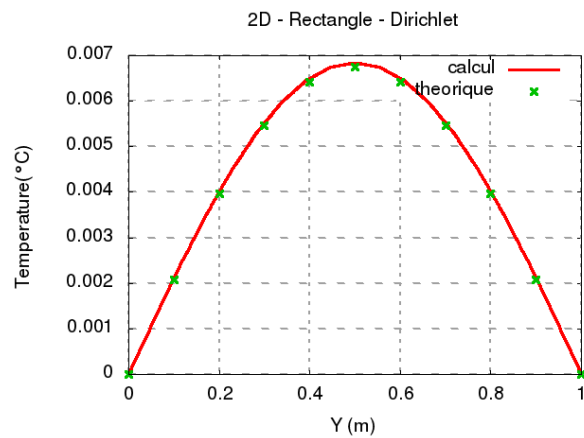
Figure 3.3: Temperature field at convergence

#### 3.4.2 Comparison calculation results / analytical values

At convergence, comparison of calculated profiles and analytical ones.

On figures 3.8 and 3.9 one compares on 2 given points the temperature calculated (steady value reached at the end of the transient) and the analytical value (exact solution of temperature).

The two nodes that were selected are: node 366 of coordinates (0.4736842,0.2564102) node 393 of coordinates (0.4736841,1.6410300)

Figure 3.4: Temperature profiles at  $Y = 0.2564$  mFigure 3.5: Temperature profiles at  $Y = 1.1795$  mFigure 3.6: Temperature profiles at  $Y = 1.64103$  m

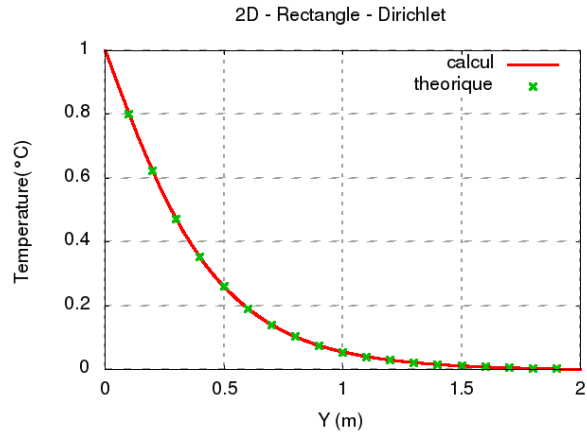


Figure 3.7: Temperature profiles at  $X = 0.4736842$  m

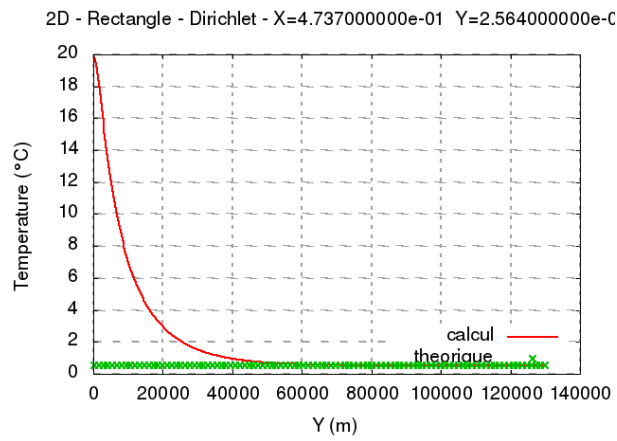


Figure 3.8: Convergence at node 366  $x=0.4737$   $y=0.2564$

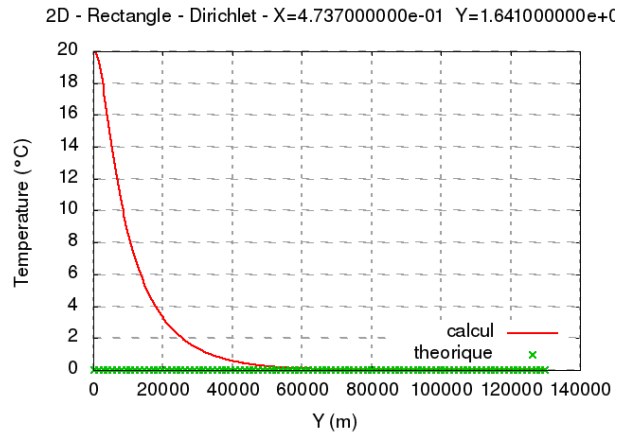


Figure 3.9: Convergence at node 393  $x=0.4737$   $y=1.6410$

Remarks :

*Error values shown on the curves correspond to the absolute value of temperature deviation between theoretical value and calculated value divided by maximum temperature deviation observed on the studied configuration. It can effectively provide a better estimate of the “relative” error committed for a given configuration. Indeed, relative error built by the ratio between temperature deviation by the temperature value at considered point maximizes totally artificially committed error when the theoretical temperature tends to 0. Conversely, a calculation made between two high temperatures would lead to estimate (again, artificially) much lower relative error.*

### 3.5 Synthesis

The elementary case RECTAN gives satisfactory solution. It allows to test particularly calculations of elementary matrices in 2D cartesian and boundary conditions of Dirichlet type.

Strictly speaking, the mesh is not necessarily optimal for this simulation. In the frame of a study, it would be preferable to densify mesh at lower level corners where the temperature field is singular and where temperature gradients are very important. Inversely, the mesh could be looser in the upper portion.

## Chapter 4

# SQUARE-H

**Characteristics :** 2D, steady state, boundary conditions of mixed type, Dirichlet and exchange coefficient.

**Objectifs :** Validation of thermal resolution inside a solid in dimension 2 for a steady state. Validation of the treatment of boundary conditions of exchange and Dirichlet type.

### 4.1 Test case description

#### 4.1.1 Geometry

Consider a square of 1m side (4.1).

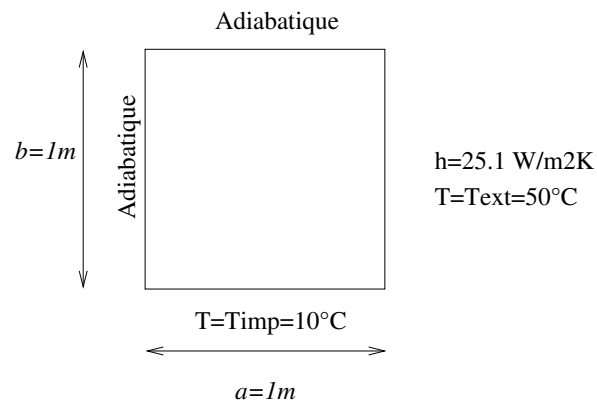


Figure 4.1: Solid domain

#### 4.1.2 Physical conditions

The solid is related to steel having following physical characteristics :

- conductivity  $k = 25.1 \text{ W/mK}$
- density  $\rho = 7700 \text{ kg/m}^3$
- specific heat  $C_p = 460 \text{ J/kgK}$

### 4.1.3 Initial conditions, boundary conditions

Initially (at  $t = 0$ ), the solid is at  $20^\circ C$ .

We impose on the lower side ( $y = 0$ ) a temperature  $T_1 = 10^\circ C$  and on the right side ( $x = 1$ ) a condition of exchange type, with  $h = 25.1 \text{ W/m}^2 K$  and the environment is at a temperature of  $50^\circ C$ .

## 4.2 Analytical solution

In case of a plate of size  $0 < x < 1$  and  $0 < y < 1$  subject to following condition : temperature  $T = T_{imp}$  in  $y = 0$  exchange condition of type  $h(T_{ext} - T)$  on side  $x = 1$  and null flux condition on others sides, temperature at point  $(x, y)$  of the plate is given by :

$$T(x, y) = T_{ext} + 2h(T_{imp} - T_{ext}) \sum_{n=1}^{\infty} \frac{\cos \alpha_n x \cosh \alpha_n (1 - y)}{[(\alpha_n^2 + h^2) + h] \cos \alpha_n \cosh \alpha_n}$$

where  $\alpha_n$  are roots of following transcendental equation :

$$\alpha_n \tan \alpha_n = 1$$

It reminds values (approximated) des 9 first roots :

$$\begin{aligned} \alpha_1 &= 0.8603 \\ \alpha_2 &= 3.4256 \\ \alpha_3 &= 6.4373 \\ \alpha_4 &= 9.5293 \\ \alpha_5 &= 12.6453 \\ \alpha_6 &= 15.7713 \\ \alpha_7 &= 18.9025 \\ \alpha_8 &= 22.0365 \\ \alpha_9 &= 25.17245 \end{aligned}$$

## 4.3 Calculations description

### 4.3.1 Mesh

Mesh has :

- 40 401 nodes with 10 201 vertex nodes
- 20 000 triangles

Nodes of the edge  $y = 0$  has reference 1, those affected by the exchange coefficient have reference 3.

We note that the used mesh is very fine. Logically, physics of the problem does not impose a so fine spatial discretization (except maybe at the bottom right corner where temperature gradients are severe). On the other hand, this mesh allows to do an informatic test with a more important number of nodes.

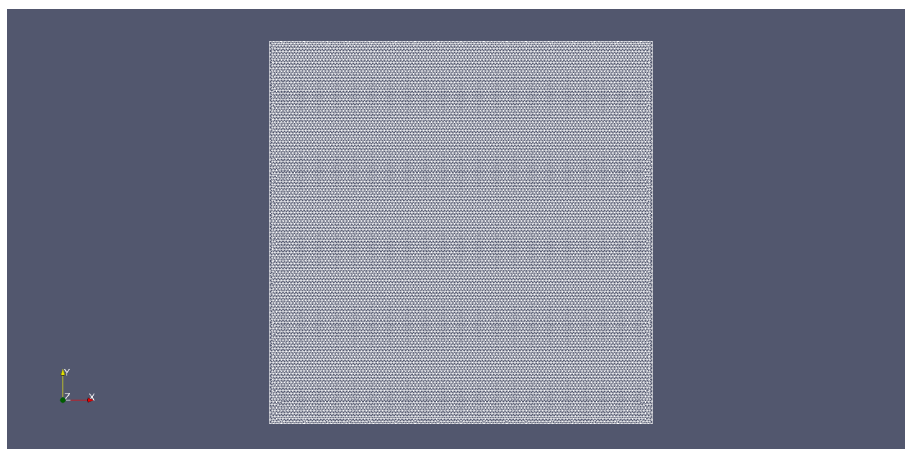


Figure 4.2: Square's mesh

## 4.4 Presentation of results

To reach the steady state, the chosen time step is high (1000s). If we wanted to simulate accurately an unstationnary evolution, it would be desirable to reduce a little bit this value.

It takes about 3.5 days (physical time) to reach the steady state.  
The calculaion needs about 300 time steps.

### 4.4.1 Thermal fields at convergence

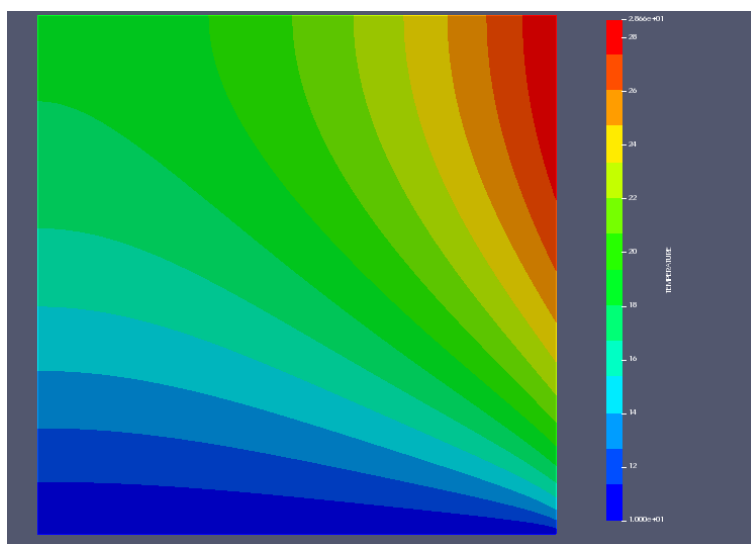


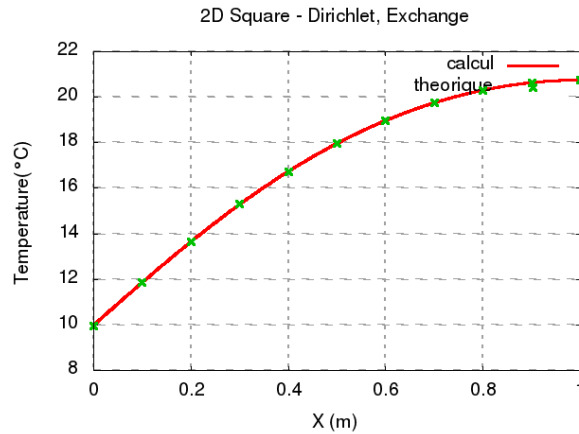
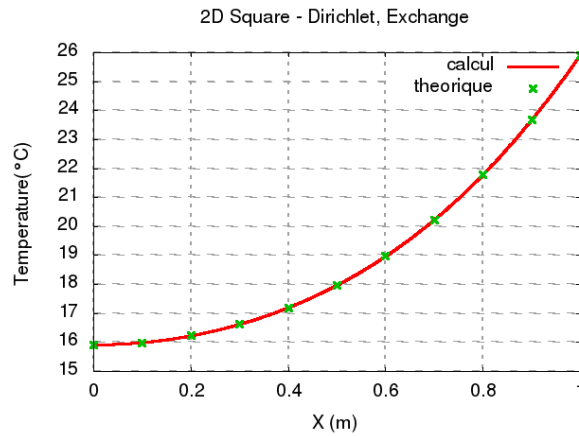
Figure 4.3: Thermal fields at convergence

### 4.4.2 Comparison calculation results / analytical value

We present 2 temperature profiles. Firts one is along the direction  $x$  (horizontal), it has ordinate  $y = 0.5$ , second one along the direction  $y$  (vertical) and has for abscisse  $x = 0.5$

Remarks :

*Prediction is obtained with a precision of about 0.05% compared to analytical solution, but note that*

Figure 4.4: Temperature profile at  $Y = 0.5$  mFigure 4.5: Temperature profile at  $X = 0.5$  m

*theoretical formula is only guaranteed to a precision of this order also, The fact that the series is truncated to the ninth term and that the transcendental equation's roots have been computed to the fourth decimal.*

## 4.5 Synthesis

The case SQUARE-H give satisfactory results. It allows to test elementary matrices's calculation in 2D cartesian on a well fine mesh but especially, it allows to test boundary conditions of exchange type. We check also that mixed conditions within one calculation (Dirichlet/exchange) are correctly taken into account.

TH retained mesh is much more fine than configuration requirement (except maybe at the bottom right corner) but this allows to test computationally a case with a number of nodes more related with those used in the industrial computing.

## Chapter 5

# RING

**Features :** 2D, steady state, boundary condition = imposed temperature

**Objectifs :** Validation of thermal resolution inside a 2D solid for a steady state. Validation of Dirichlet conditions's processing. Influence of mesh's fineness.

### 5.1 Test case description

#### 5.1.1 Geometry

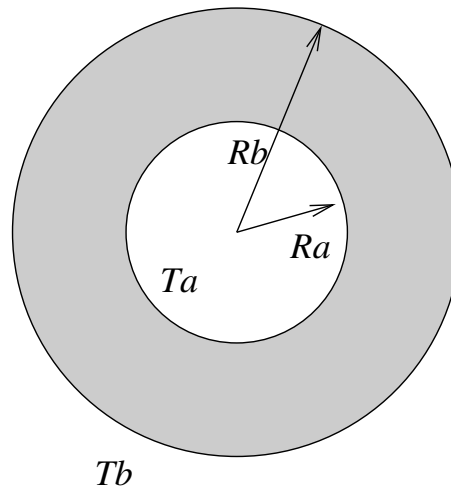


Figure 5.1: Solid domain

We consider a ring whose dimension are :

- inner radius  $R_a = 0.5m$
- outer radius  $R_b = 1m$

#### 5.1.2 Physical conditions

The solid is related to steel having following physical characteristics :

- conductivity  $k = 25 W/mK$
- density  $\rho = 7700 kg/m^3$
- specific heat  $C_p = 460 J/kgK$

### 5.1.3 Initial conditions, boundary conditions

Initially (at  $t = 0$ ), the solid is at  $20^{\circ}C$ .

We impose on the inside of the ring a temperature  $T_a = 10^{\circ}C$  and on the outside a temperature  $T_b = 50^{\circ}C$ .

## 5.2 Analytical solution

In case of a small radius ring  $R_a$  and large radius  $R_b$ , which inside temperature is imposed at  $T_a$  and outside temperature at  $T_b$  we obtain, at steady state, the temperature to a point located at a radius  $r$  as follows :

$$T(r) = \frac{T_a \log\left(\frac{R_b}{r}\right) + T_b \log\left(\frac{r}{R_a}\right)}{\log\left(\frac{R_b}{R_a}\right)}$$

## 5.3 Calculations description

### 5.3.1 Mesh

Two meshes have been made in order to test influence of meshes size on results.

The coarse mesh has :

- 2 888 nodes with 760 vertex nodes,
- 1 368 triangles.

For the fine mesh, we have divided the meshes size by 2. It has :

- 12 168 nodes dont 3 120 vertex nodes,
- 5 928 triangles.

In both cases, internal boarder nodes has reference 1, those of external boarder reference 2, others reference 0.

## 5.4 Presentation of results

Steady state is obtained after about 1 hour of physical time. For both meshes, we have used a time step equal to 100 seconds. For the coarse mesh, convergence has been reached after nearly 350 time steps. For the fine mesh, steady state is obtained after nearly 350 time steps.

### 5.4.1 Thermal fields inside the ring

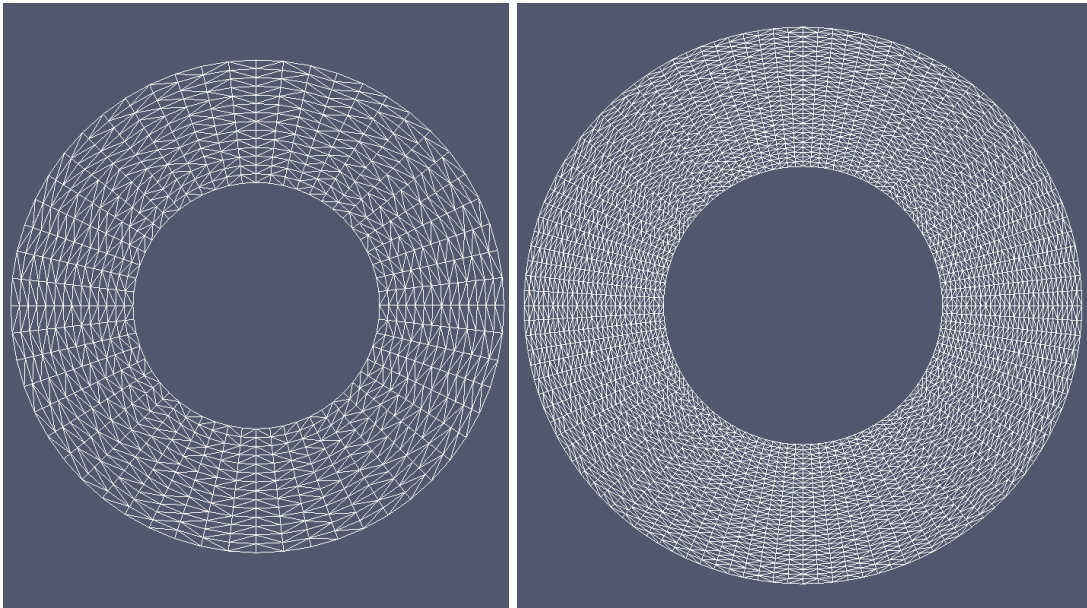


Figure 5.2: Coarse and fine meshes

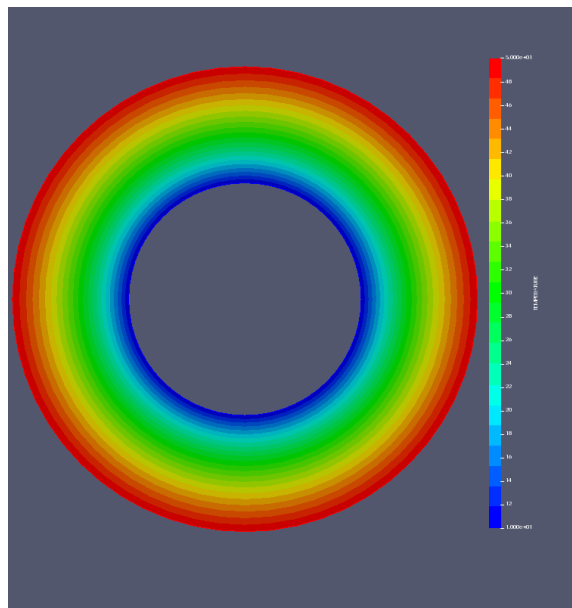


Figure 5.3: Converged thermal field

### 5.4.2 Comparison calculation results / analytical value

Comparisons between calculated values and analytical values are made along a radius of the ring.

Figure 5.4 presents a comparison between calculated and analytical profiles for calculation with the coarse mesh (on the left) and with the fine mesh (on the right).

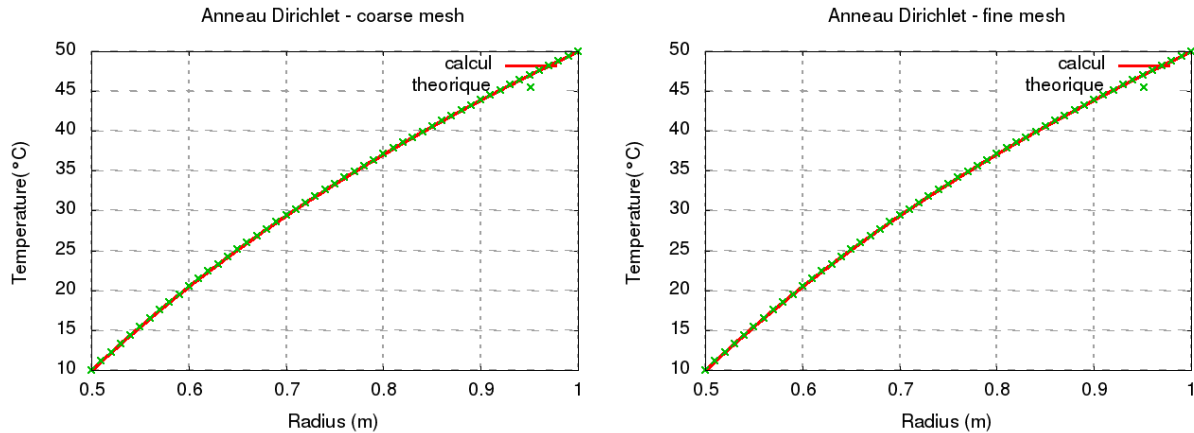


Figure 5.4: Theoretical and calculated profiles along a radius

#### Study of calculation's convergence

Following figures show evolution of temperature in 2 points given. Results are presented in the case of coarse and fine meshes. The two chosen nodes are :

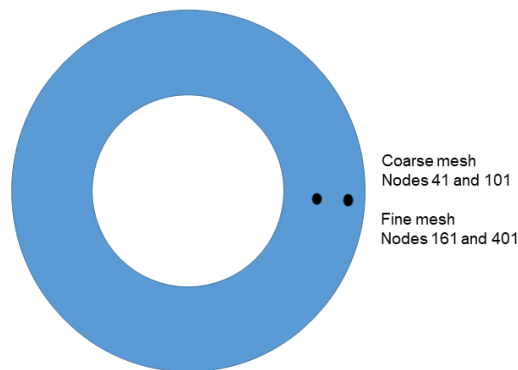


Figure 5.5: Positions of nodes for convergence study

Coarse mesh : used nodes's number

- Node 41 of coordinates (0.61111, 0.)
- Node 101 of coordinates (0.77777, 0.)

Fine mesh : used nodes's number

- Node 161 of coordinates (0.60526, 0.)
- Node 401 of coordinates (0.76315, 0.)

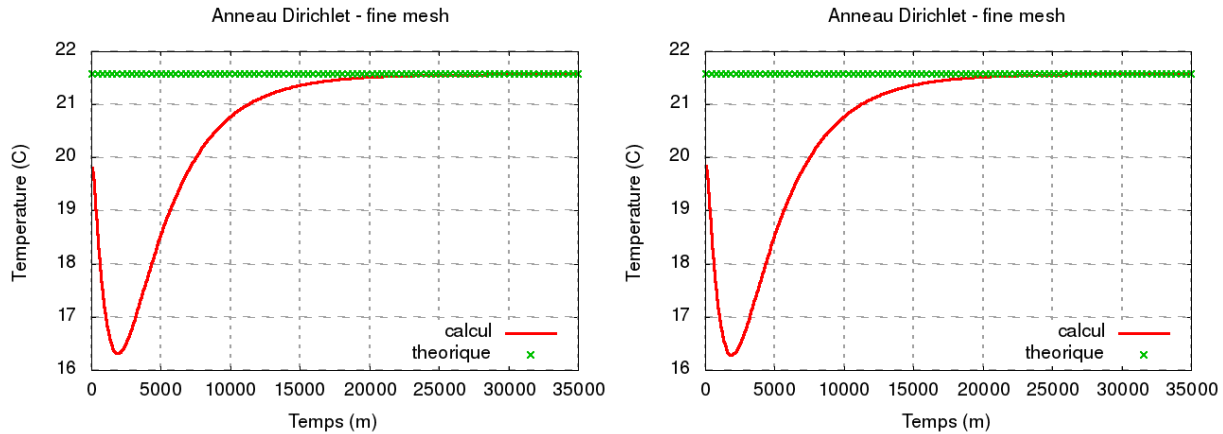


Figure 5.6: Study of convergence (Radius  $\approx 0.61$ )

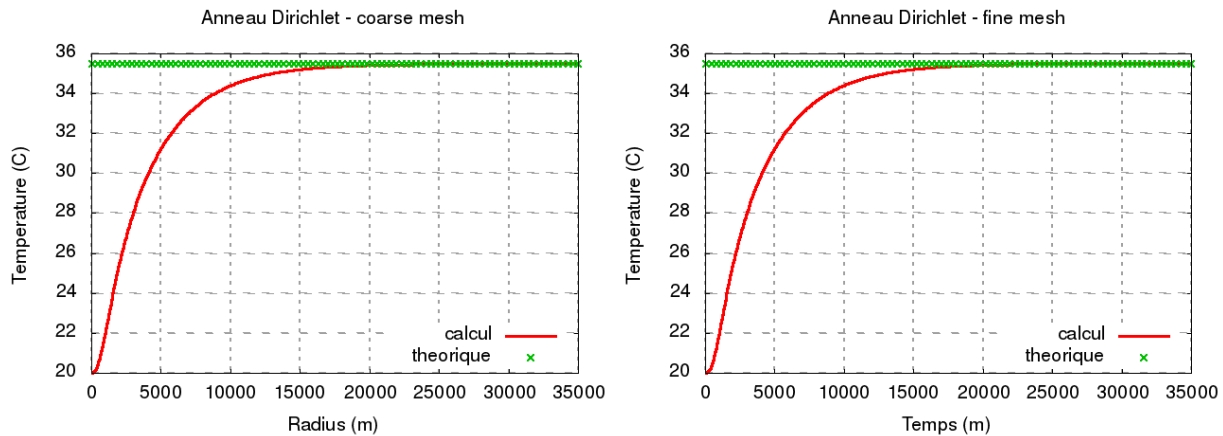


Figure 5.7: Study of convergence (Radius  $\approx 0.77$ )

Remarks :

*Like for previous configuration, error values mentionned on curves correspond to the absolute value of temperature gap between theoretical value and calculated value divided by the maximum observed temperature gap on the studied configuration.*

## 5.5 Synthesis

The case ANNEAU gives satisfactory results. We find by calculation, the cylindrical nature of the solution (whereas elementary matrices are of course cartesian).

Objective of this configuration is primarily to test the influence of mesh. The results confirm that calculated solution improves the mesh is refined.

In the present case, error's origin (which still remains low, a few thousandths to one hundredth degree on a temperature difference of about 40 °C) might arise from the fact that the spatial discretization implies faceting edges of cylinders. Perimeters on which we impose the boundary conditions are no longer strictly identical to the theoretical case. First approach, if we consider a perimeter cut into  $n$  edge facets, the relative error committed on the perimeter is about :

$$\frac{\pi^2}{6n^2} \left[ 1 - \frac{\pi^2}{20n^2} \right]$$

Similarly, error between the rope and the arc of the theoretical case may cause a position error about :

$$\frac{\pi^2}{n^2} \left[ 1 - \frac{\pi^2}{24n^2} \right]$$

In the case of the ring, the numerical implementation with a cylinder cut in 76 facets give relative errors about  $2.84710^{-4}$  and  $1.710^{-3}$  respectively for perimeter and positioning.

## Chapter 6

# RING-H

**Features :** Stationary 2D, boundary conditions of exchange coefficient type

**Objectives :** Validation of thermal resolution inside a 2D solid in a stationary frame. Validation of boundary conditions's processing of exchange coefficient type.

### 6.1 Test case description

Geometry and physical conditions of this case are identical to those of test case “ring”. Only boundary conditions are different.

#### 6.1.1 Geometry

We consider a ring whose inner radius is  $R_a = 0.5\text{ m}$  and outer radius is  $R_b = 1\text{ m}$ .

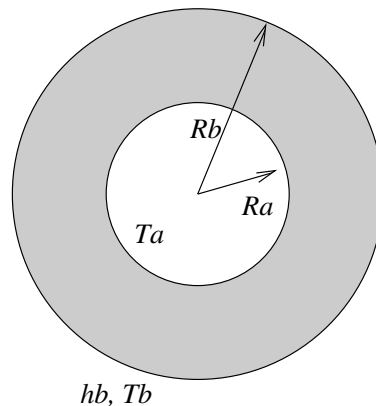


Figure 6.1: Solid domain

#### 6.1.2 Physical conditions

The solid is related to steel having following physical characteristics:

- conductivity  $k = 25\text{ W/mK}$
- density  $\rho = 7700\text{ kg/m}^3$
- specific heat  $C_p = 460\text{ J/kgK}$

### 6.1.3 Initial conditions, boundary conditions

Initially (at  $t = 0$ ), the solid is at  $20^\circ C$ .

We impose on the inside of the ring a temperature of  $10^\circ C$  and on the outside an exchange coefficient of  $h = 10 W/m^2K$  and an outside temperature of  $50^\circ C$ .

## 6.2 Analytical solution

In case of a small radius ring  $R_a$  and large radius  $R_b$ , which inside temperature is imposed at  $T_a$  and having on its external surface a exchange coefficient  $h_b$  and an external temperature  $T_b$ , we obtain at steady state the temperature at a point located at a radius  $r$  as follows :

$$T(r) = \frac{T_a \left( 1 + h_b R_b \log \left( \frac{R_b}{r} \right) \right) + T_b h_b R_b \log \left( \frac{r}{R_a} \right)}{1 + h_b R_b \log \left( \frac{R_b}{R_a} \right)}$$

## 6.3 Calculations description

### 6.3.1 Mesh

The mesh (identical to the one of case “ring” with coarse mesh) has :

- 2 888 nodes with 760 vertex nodes,
- 1 368 triangles.

Nodes of internal border have 1, those of the external border have reference 2, others have reference 0.

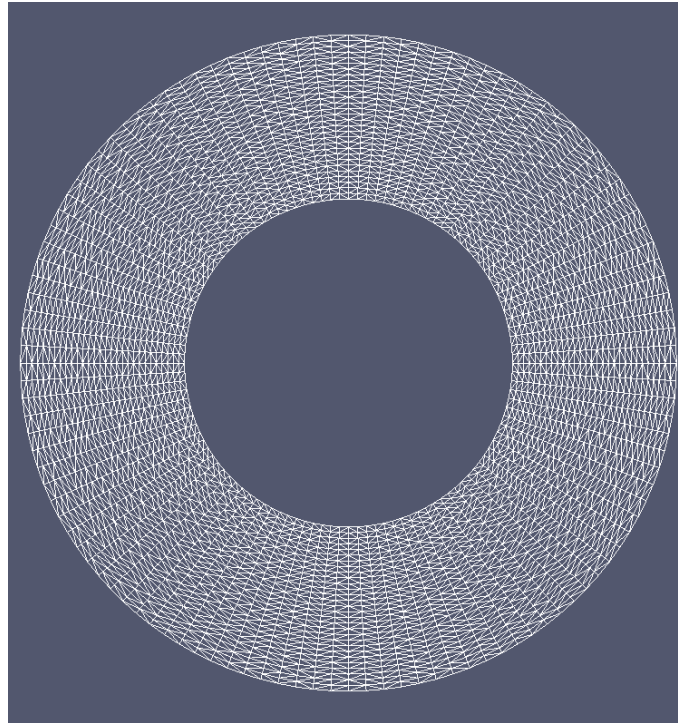


Figure 6.2: Mesh

## 6.4 Presentation of results

Steady state is obtained after nearly 1.5 days of physical time.

We have used a time step equal to 500 secondes.  
Convergence has been reached after nearly 250 time steps.  
Calculation needed 10.0 seconds on SGI station.

### 6.4.1 Thermal fields inside the ring

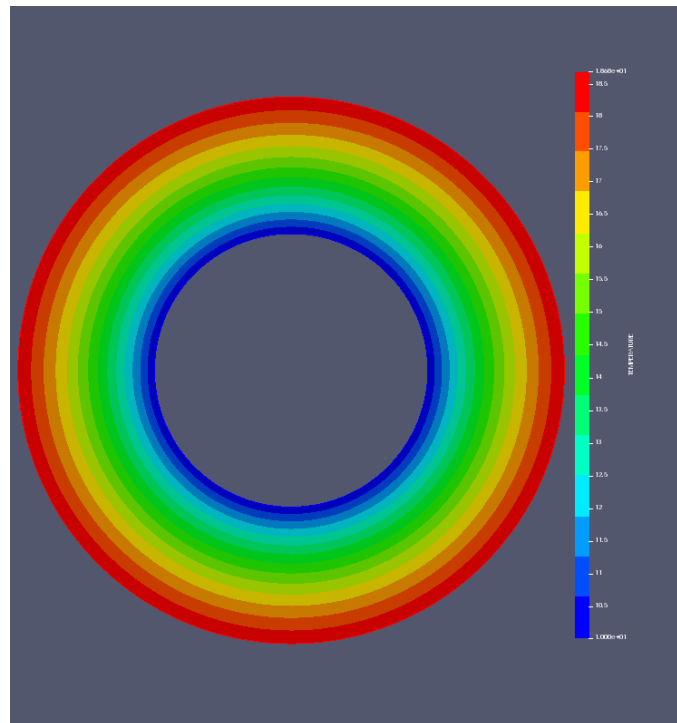


Figure 6.3: Converged thermal field

### 6.4.2 Comparison calculation results / analytical value

Comparisons between calculated values and analytical values (figure 6.4) are made along a radius of the ring.

#### Study of calculation's convergence

Figures 6.5 at 6.7 show the temperature's evolution in 3 points given :

- Node 41 of coordinates (0.611111)
- Node 101 of coordinates (0.77777, 0.)
- Node 181 of coordinates (1., 0.)

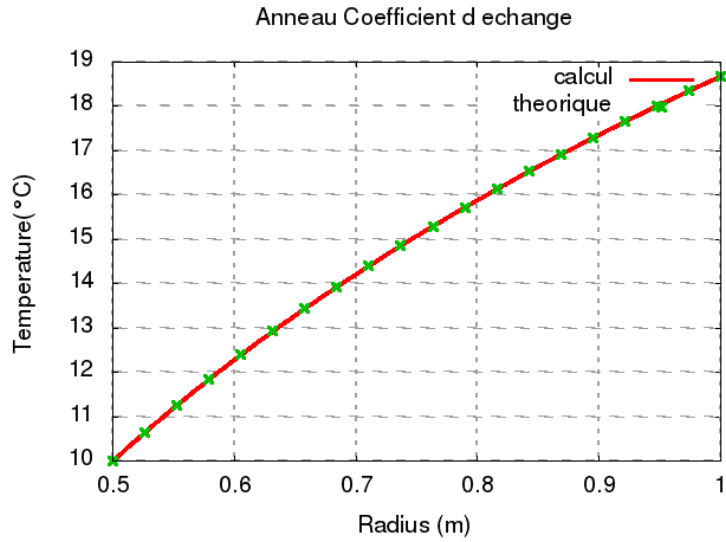


Figure 6.4: Theoretical profiles and calculated along a radius

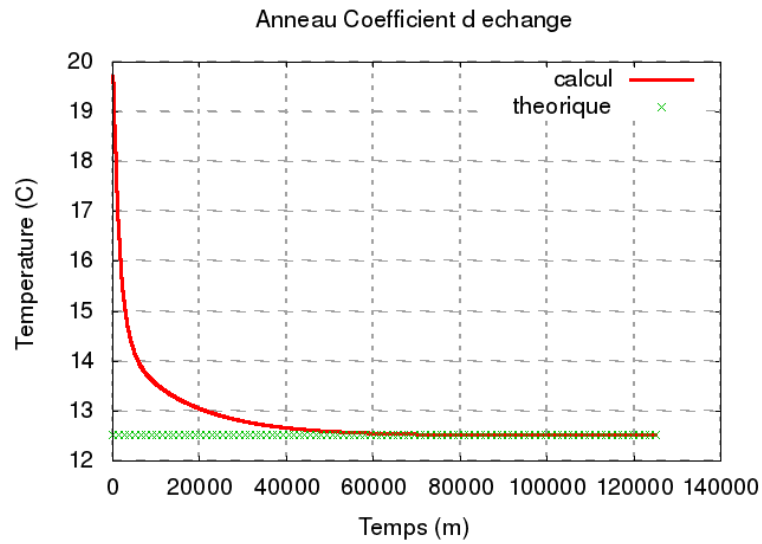
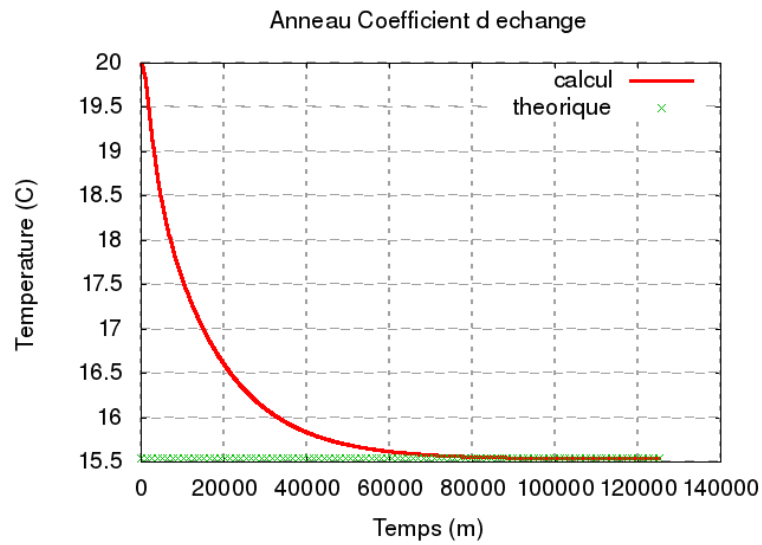
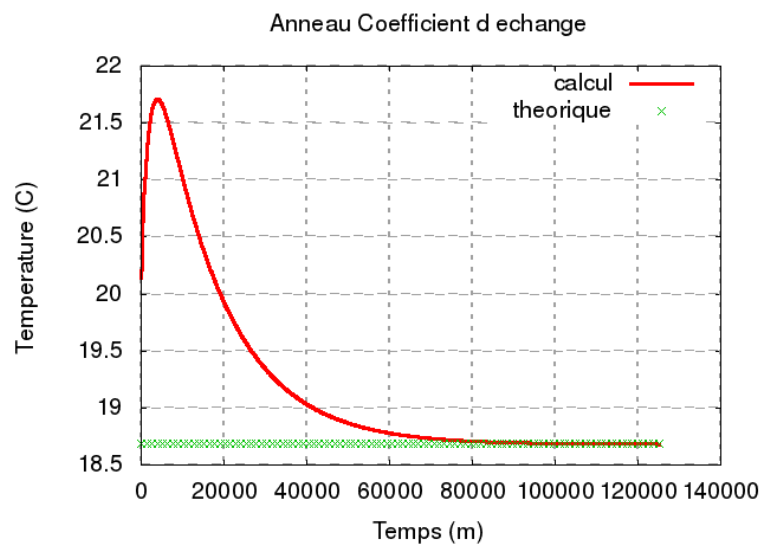


Figure 6.5: Convergence at R=0.611111

Figure 6.6: Convergence at  $R=0.77777$ Figure 6.7: Convergence at  $R=1$ .

Remarks :

*Like for previous configurations, error values mentionned on curves correspond to the absolute value of temperature gap between theoretical value and calculated value divided by the maximum observed temperature gap on the studied configuration.*

## 6.5 Synthesis

Configuration RING-H is considered satisfactory. This configuration checks a case with only heat exchange boundary conditions : temperatures at the boundary remain unknown values of the problem. The same remarks regarding the facettisation of the border apply : it should however relativize this “approximation” whose importance is still minimal. Indeed, one must be aware in an industrial configuration, the data of the problem (geometry, boundary conditions, materials behavior, etc...) are almost never known with the precision level mentioned here.

## Chapter 7

# SPHERE

**Characteristics :** Unsteady 3D (here represented by a discretization 2D), boundary conditions of Dirichlet type.

**Objectives :** Validation thermal resolution inside a solid in 2D in an unsteady frame. Validation of axisymmetric modeling. Validation of the treatment of Dirichlet's conditions.

### 7.1 Test case description

#### 7.1.1 Geometry

We consider a solid sphere of radius :  $R_a = 0.5m$

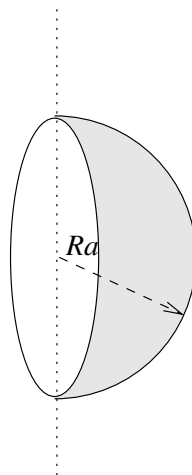


Figure 7.1: Solid domain

#### 7.1.2 Physical conditions

The solid is related to steel having following physical characteristics :

- conductivity  $k = 25 W/mK$
- density  $\rho = 7700kg/m^3$
- specific heat  $C_p = 460J/kgK$

### 7.1.3 Initial conditions, boundary conditions

Initially (at  $t = 0$ ), the solid is at  $0^\circ C$ .

We impose on the outer surface a temperature  $T_a = 1^\circ C$

Since the modeling is 2D axisymmetric, one must impose a boundary condition along the inside diameter of the sphere. A null flux condition will represent the 3D character of the case.

## 7.2 Analytical solution

In the case of a sphere of radius  $R_a$ , we remind that the analytical solution is written for a given radius  $r$  and  $t$  :

$$T(r) = T_a + \frac{2R_a T_a}{\pi r} \sum_{n=0}^{\infty} \frac{(-1)^n}{n} \sin\left(\frac{n\pi r}{R_a}\right) e^{-\frac{kn^2\pi^2 t}{R_a^2}}$$

A specific expression of this formula exists for the center of the sphere (obtained as limit  $r \rightarrow 0$  of the previous expression).

$$T(0) = T_a + 2T_a \sum_{n=1}^{\infty} (-1)^n e^{-\frac{kn^2\pi^2 t}{R_a^2}}$$

## 7.3 Calculation description

### 7.3.1 Mesh

The mesh is realised in 2D, it uses axisymmetry property of the problem, this leads to mesh only a slice of sphere.

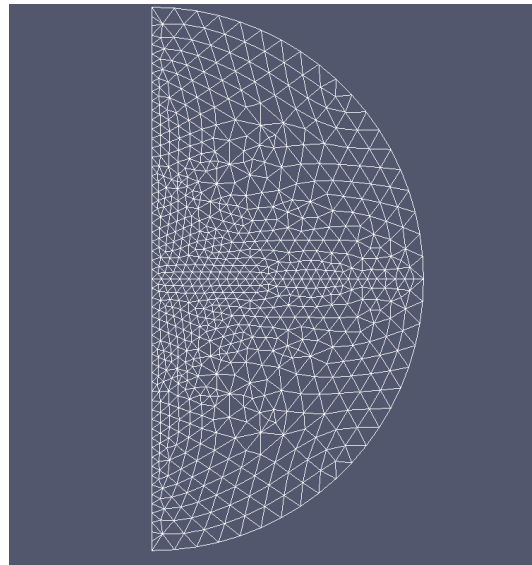


Figure 7.2: Mesh

The mesh has :

- 1 407 nodes with 369 vertex,
- 670 triangles.

The nodes of the sphere's diameter ( $x=0$ ) have the reference 1, those of the outer border reference 2, others reference 0.

## 7.4 Presentation of results

We have performed calculation with a time step equal to 10 seconds, which allows to check the quality of prediction of thermal transient in an axisymmetric coordinate system.

Convergence has been reached after about 50000 physical seconds (about 14 hours), representing 5000 time steps.

### 7.4.1 Temperature field inside the sphere

From time  $t = 0$ , a progressive warming of the sphere appear. So expected isotherms are concentrically. We present here a half section of the sphere after 1000, 2000, 5000 et 10000 seconds.

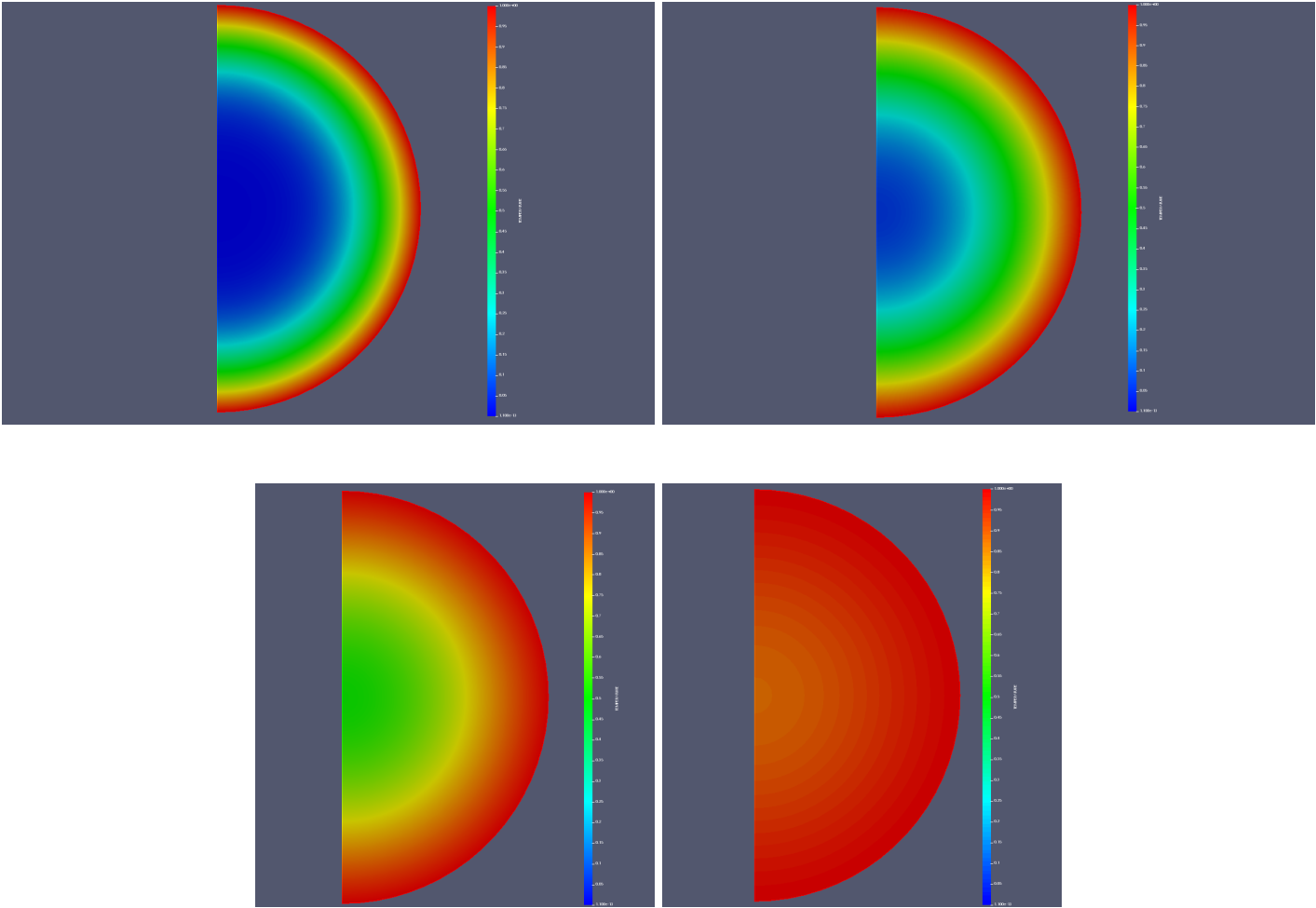


Figure 7.3: Temperature field at four moments

### 7.4.2 Comparison calculation results / analytical values

Comparisons between calculated values of temperature and analytical values are made along a radius of the sphere at different moments (100s, 1000s, 2500s, 5000s, 10000s, 20000s, 50000s).

The analysed profile is defined as follows for the studied mesh :

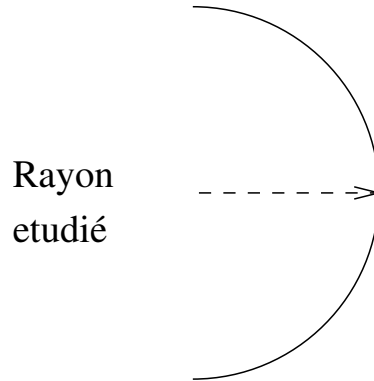


Figure 7.4: Profiles used for the results's evaluation

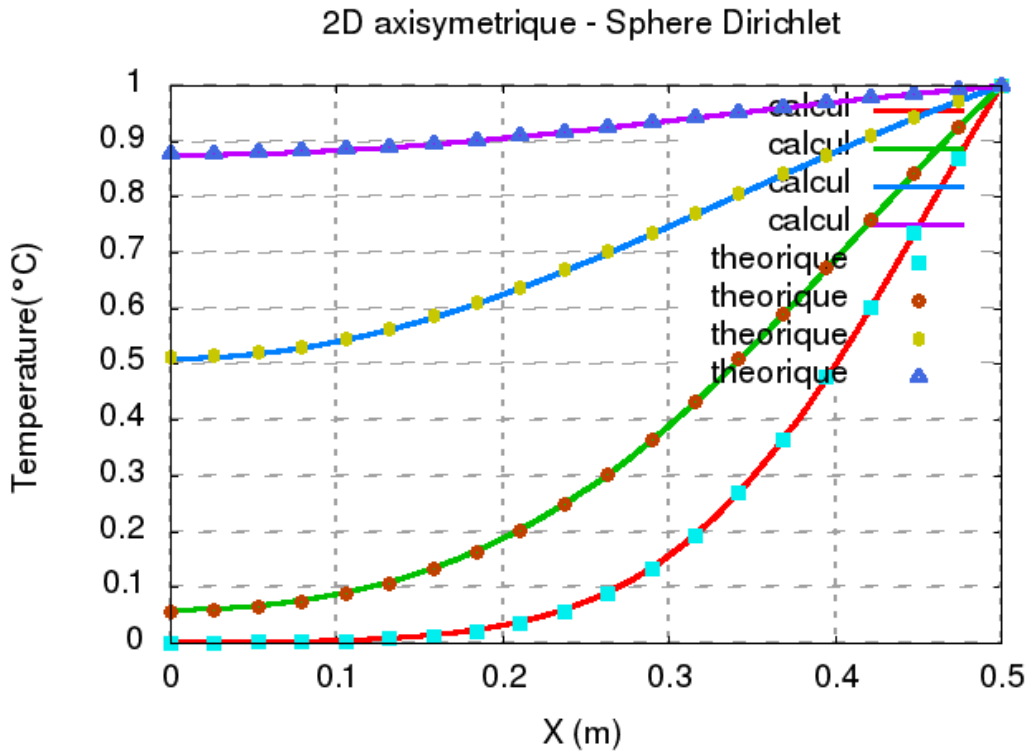


Figure 7.5: Theoretical and calculated profiles along a radius

Remarks :

*On the first curve, we note a more angular profile. A use of a finer mesh would already lead to obtain a curve closer to theoretical values.*

### Study of calculation's convergence

The figure 7.6 shows evolution of temperature at the center of the sphere. We note the good comparison of calculated transient with the theoretical transient.

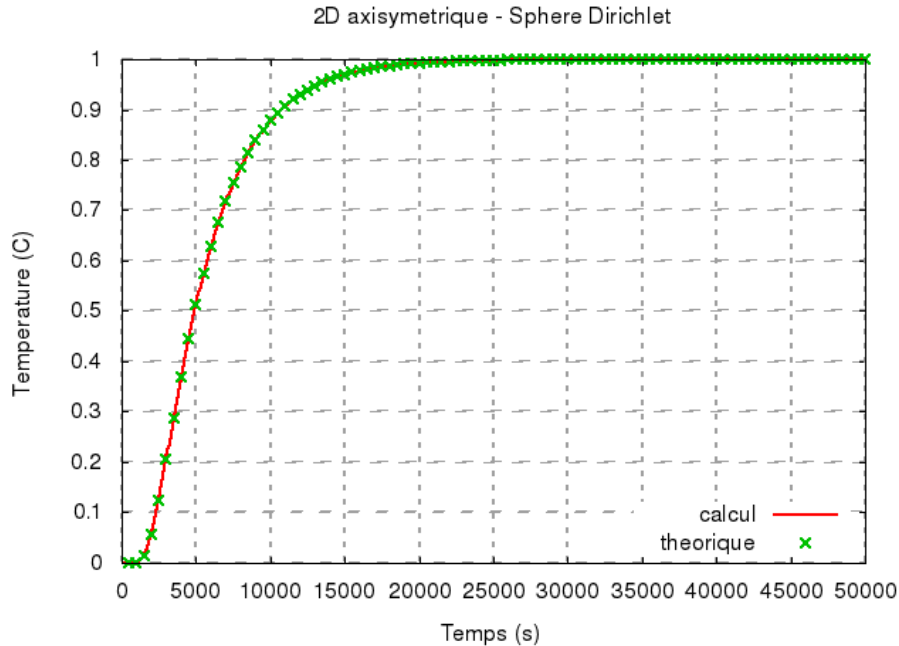


Figure 7.6: Study of the convergence in time

## 7.5 Synthesis

Results obtained with on the test case SPHERE are considered satisfactory. This test has particularly allowed to validate the construction of the elementary matrices for an axisymmetric coordinate system. The temperature field during transient is well concentric (corresponds well to the fact that this is a 1D problem in spherical coordinates). We also searched through this configuration to evaluate the quality of unsteady treatment done in SYRTHES. We see in figure 7.6 a good agreement between exact temporal to the center of the sphere and that obtained numecally. It should be noted that take a time step much higher lead to an error on evaluation of transient. If we are interested in more precision in the first instants of transient near the skin, where gradients are the most intense during transient, the mesh could be considered as insufficiently refined in this zone, and the chosen time step too high.

## Chapter 8

# BRICK

**Characteristics : 3D, transient**

**Objectives :** Validation of thermal resolution inside a solid for a 3D transient frame.

### 8.1 Test case description

#### 8.1.1 Geometry

Consider a brick whose dimensions (in meters) are following :

- $-0.4 < x < 0.4$
- $-0.2 < y < 0.2$
- $-0.1 < z < 0.1$

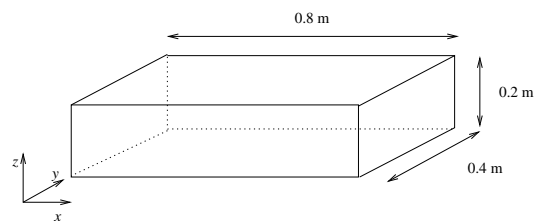


Figure 8.1: Calculation domain

#### 8.1.2 Physical conditions

The solid is related to steel having following physical characteristics :

- conductivity  $k = 25 \text{ W/mK}$
- density  $\rho = 7700 \text{ kg/m}^3$
- specific heat  $C_p = 460 \text{ J/kgK}$

#### 8.1.3 Initial conditions, boundary conditions

Initially (at  $t = 0$ ), the solid is at  $0^\circ\text{C}$ .

We impose on the whole surface a temperature of  $50^\circ\text{C}$ .

## 8.2 Analytical solution

Consider a brick whose initial temperature is  $T_0 = 0^\circ C$  temperature on the surface is imposed at  $T_1 = 50^\circ C$  and dimensions are :

- $-a < x < a$
- $-b < y < b$
- $-c < z < c$

Temperature inside the solid is given according to the instant  $t$  by the following analytical formula.

$$T = T_1 - \frac{64 T_1}{\pi^3} \sum_{l=0}^{\infty} \sum_{n=0}^{\infty} \sum_{m=0}^{\infty} \frac{(-1)^{l+m+n}}{(2l+1)(2m+1)(2n+1)} \cos\left(\frac{(2l+1)\pi x}{2a}\right) \cos\left(\frac{(2m+1)\pi y}{2b}\right) \cos\left(\frac{(2n+1)\pi z}{2c}\right) e^{-\alpha_{lmn} t}$$

avec

$$\alpha_{lmn} = \frac{k}{\rho C_p} \frac{\pi^2}{4} \left[ \frac{(2l+1)^2}{a^2} + \frac{(2m+1)^2}{b^2} + \frac{(2n+1)^2}{c^2} \right]$$

## 8.3 Calculations description

### 8.3.1 Mesh

The mesh has :

- 102695 nodes with 13824 vertex nodes,
- 71346 tetrahedra.

Border nodes have reference 1 others, reference 0.

## 8.4 Presentation of results

Since we are interested in a transient phenomenon, the time step is 1 second in initial phase where temperature gradients are important then 10 s until convergence.

### 8.4.1 Thermal field inside the brick

Thermal field is presented at time  $t=1000$  seconds.

Following the calculation temperature of the brick is of course constant and equal to  $50^\circ C$ .

### 8.4.2 Comparison calculated results / analytical value

We present transient evolution of the temperature profile along a path  $y$ . Initially only the points belonging to the edges of the brick are set to  $50^\circ C$ , temperature in the other parts of the solid is closed to  $0^\circ C$ . Then progressively, temperature in the center of the brick increases. After nearly 4000 seconds of real time, the temperature of the brick is  $50^\circ C$  at any point.

Following figures show some of these profiles and compare them to theoretical profiles, obtained with the previously given analytical formula. For reasons of clarity, results are presented on 2 figures with separate scales, but note that the right one is the temporal continuity of the left one (however, the scales have been adapted).

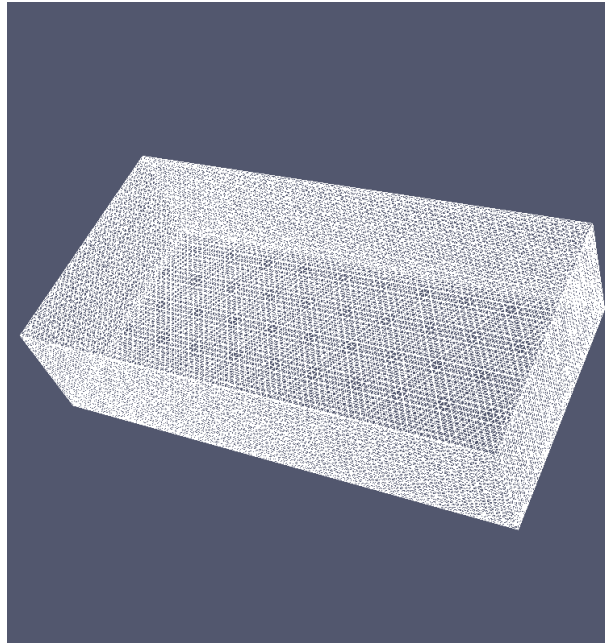


Figure 8.2: Mesh

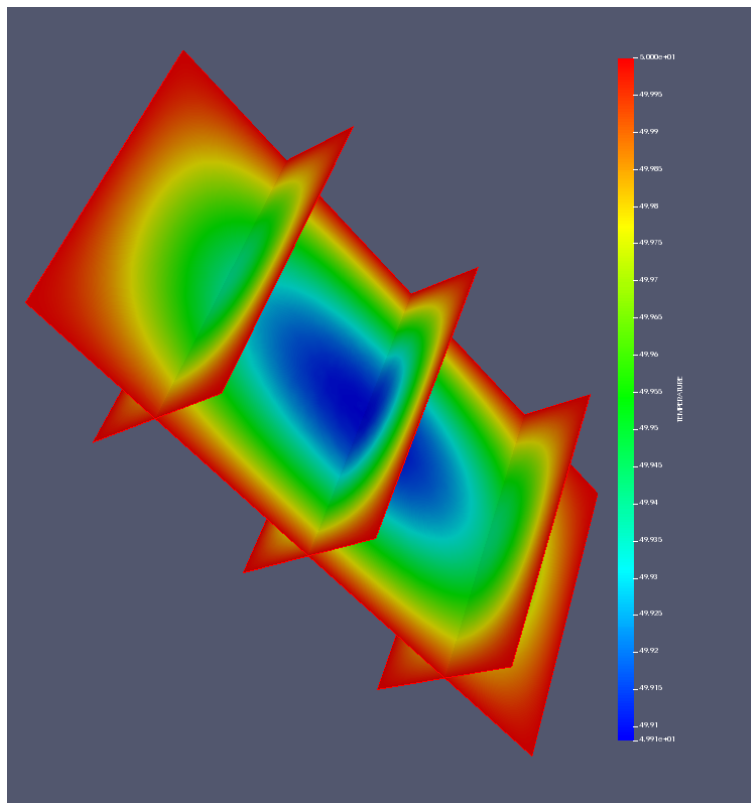


Figure 8.3: Thermal field at 1000 s

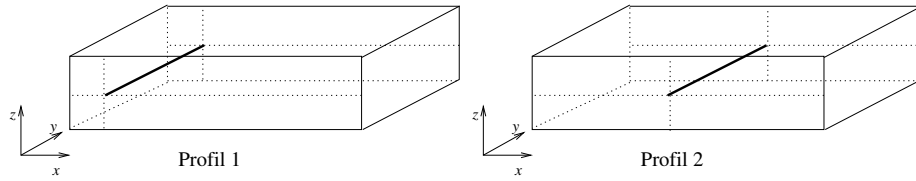


Figure 8.4: Position of the 2 studied profiles

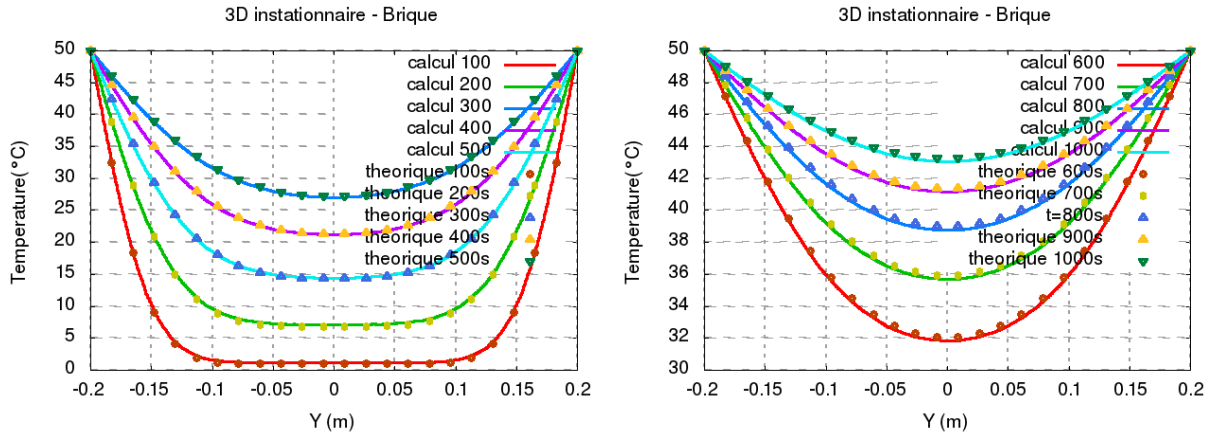


Figure 8.5: Profile 1 - Comparison calculated results / analytical values

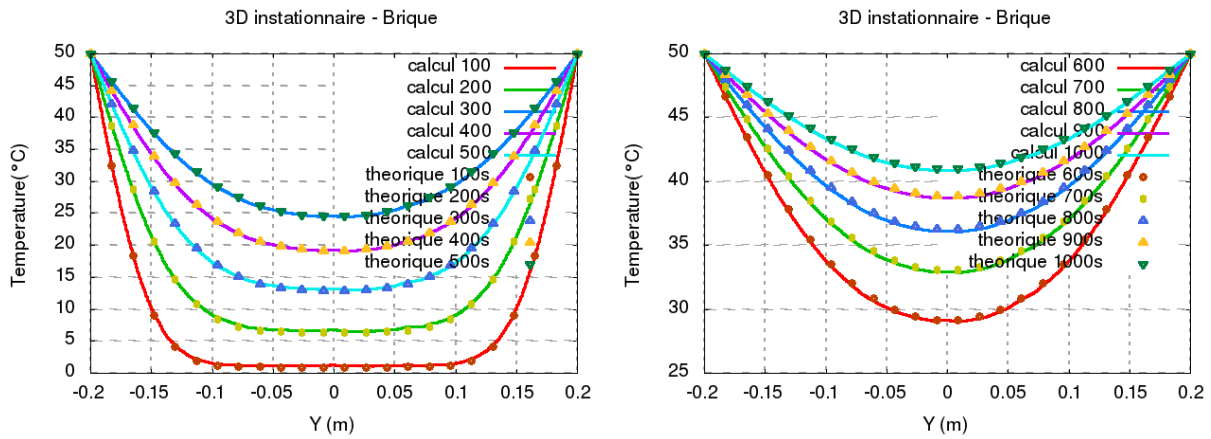


Figure 8.6: Profile 2 - Comparison calculated results / analytical values

Finally, we compare analytical values and calculated of temperature over time, in two given points :

- Node 7116 of coordinates  $(-0.2683, -0.869 \cdot 10^{-2}, -0.909 \cdot 10^{-2})$
- Node 7500 of coordinates  $(-0.8511 \cdot 10^{-2}, -0.869 \cdot 10^{-2}, -0.909 \cdot 10^{-2})$

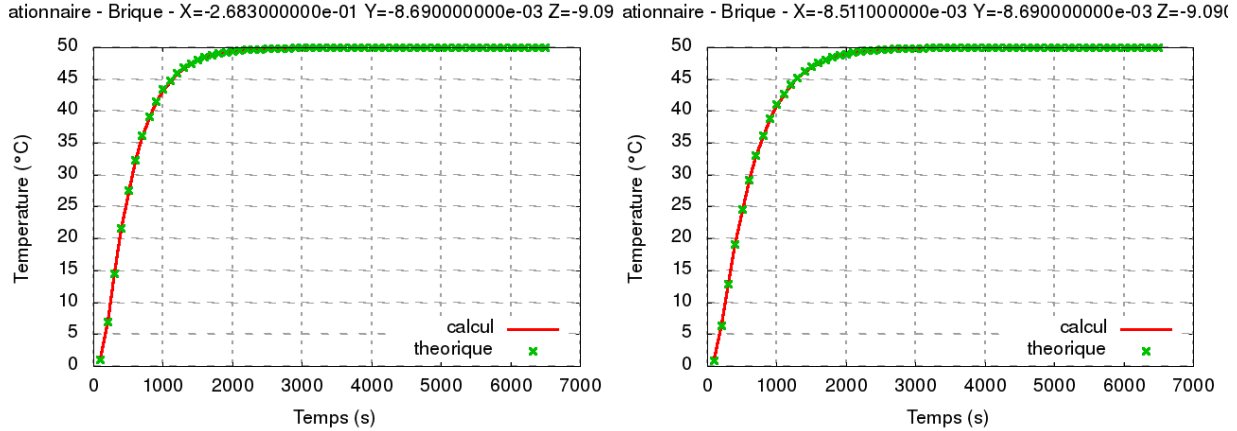


Figure 8.7: Thermal transient in 2 points

The comparison between calculated temperatures, and analytical solution is better for node 7500. This can be explained by the fact that this point is closer to the center of the brick. Then, warming is more even.

To obtain such a good precision on the first point, a smaller value of the time step would be better (the error is a function of time of  $\delta t$ ).

## 8.5 Synthesis

Results obtained with the test case BRICK are considered satisfactory. This test case allowed to validate construction of 3D elementary matrices, boundary conditions of Dirichlet in 3D, as consideration of transient aspect. It should be noted that this configuration is really 3D, in the sense that temperature gradients aren't aligned with any preferred axis. Like for some configurations already presented, it should be noted that in the case of industrial studies, it would be preferable to focus on mesh's refinement on the edges of the domain, where the temperature gradients seen during the transient are the most important.

Part II

RADIATION

## Chapter 9

# Introduction

Radiation is the second type of energy transfer which is taken into account in SYRTHES. In the theoretical SYRTHES [4] manual, you will find explanations about theoretical equations, approximations and numerical methods.

Using the radiosity method, a balance of energy is written for each triangle of the radiation mesh

$$J_i - \rho_i \sum_{j=1}^n F_{ij} J_j = M_i \quad \forall i$$

where  $J_i$  is the radiosity of the face  $i$ ,  $M_i$  the emittance and  $\rho_i$  the reflectivity.  $F_{ij}$  is the view factor between the faces  $i$  and  $j$ . It is only dependent on the geometry and the value is constant during the calculation (when geometry doesn't move).

Note that  $F_{ij}$ , a quadruple integral, can be physically interpreted as the proportion of illuminating starting from  $j$  and going to  $i$ .

Concerning the radiation module, you have to check :

- the surfacic mesh(es)
- the accuracy of view factors calculation (important step because it will be the way how energy will be divided),
- the radiation solver,
- conduction/radiation coupling,

Following test cases will show the quality of these different steps.

The first test cases are elementary : they check the view factors calculation. As they seem simple, they represent the different configurations one can find in an industrial case.

Concerning the conduction/radiation coupling, one can note that only stationary states have been tested. Numerical resolution of transient configurations are however easy (in fact, with SYRTHES a stationary state is always computed/achieved as the converged state of a transient calculation) but analytical solutions could not have been determined by the authors.

## Chapter 10

# View factors

The validation of the view factors calculation has been made with test-cases for which analytical solutions exist [14],[5].

Moreover, in case of closed cavity, sum of all the view factors must be equal to 1. This property allows to have an evaluation of the accuracy of the global calculation, even in case of complex geometries.

### 10.1 View factors in dimension 3

We present 3 cases :

- view factor between 2 face to face rectangular faces,
- view factor between 2 coincident faces joined along one edge and with an angle  $\theta$ ,
- view factors in a cylinder.

### 10.1.1 View factor between 2 face to face rectangular faces

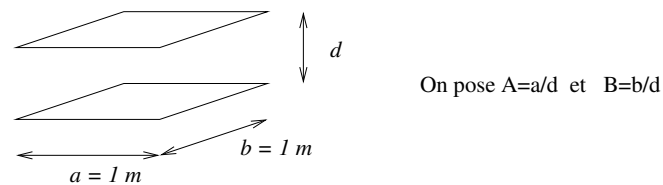


Figure 10.1: 2 face to face rectangular faces at a distance  $d$

$$F_{12} = \frac{2}{\pi AB} \left[ \log \sqrt{\frac{(1+A^2)(1+B^2)}{1+A^2+B^2}} + A\sqrt{1+B^2} \arctan \frac{A}{\sqrt{1+B^2}} \right. \\ \left. + B\sqrt{1+A^2} \arctan \frac{B}{\sqrt{1+A^2}} - A \arctan A - B \arctan B \right]$$

Results are :

Distance $d$	Solution analytique	SYRTHES
10	0.00316205683	0.00316205683
1	0.19982489569	0.19982489569
0.1	0.82699452239	0.82699452297
0.01	0.98041660292	0.98041660542
0.001	0.99800563190	0.99800606681
0.0001	0.99980007097	0.99980026059

We notice that the precision is better as the distance is high. This comes from the fact that the function to integrate includes the square of the inverse of the distance between two points crossing each facet. This distance varies much more when the two facets are close.

Remarque :

*It should be noted that this case is obtained by re-cutting each facet into 2 triangles (the only type of element allowed in 3D) then applying the additivity rules of the view factors.*

### 10.1.2 Case of 2 facets making an angle $\Theta$

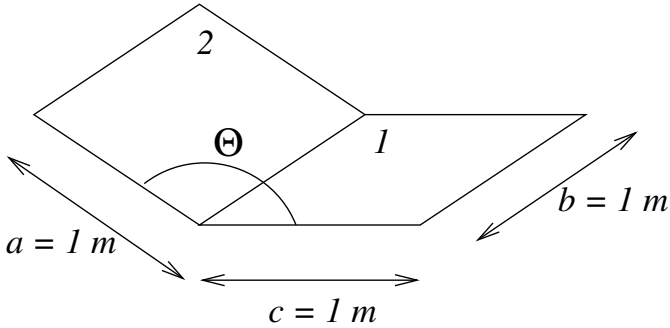


Figure 10.2: 2 facets making an angle  $\Theta$

On pose

$$A = \frac{a}{b} \quad B = \frac{c}{b} \quad C = A^2 + B^2 - 2AB \cos \Theta$$

$$\begin{aligned}
 F_{12}\pi B &= -\frac{\sin 2\Theta}{4} \left[ AB \sin \Theta + \left(\frac{\pi}{2} - \Theta\right)(A^2 + B^2) \right. \\
 &\quad \left. + B^2 \tan^{-1} \frac{A - B \cos \Theta}{B \sin \Theta} + A^2 \tan^{-1} \frac{B - A \cos \Theta}{A \sin \Theta} \right] \\
 &+ \frac{\sin^2 \Theta}{4} \left[ \left(\frac{2}{\sin^2 \Theta} - 1\right) \log \frac{(1 + A^2)(1 + B^2)}{1 + C} \right. \\
 &\quad \left. + B^2 \log \frac{B^2(1 + C)}{(1 + B^2)C} + B^2 \log \frac{A^2(1 + A^2)\cos 2\Theta}{C(1 + C)\cos 2\Theta} \right] \\
 &+ B \tan^{-1} \frac{1}{B} + A \tan^{-1} \frac{1}{A} - \sqrt{C} \tan^{-1} \frac{1}{\sqrt{C}} \\
 &+ \frac{\sin \Theta \sin 2\Theta}{2} \sqrt{1 + A^2 \sin^2 \Theta} \\
 &\quad \left[ \tan^{-1} \frac{A \cos \Theta}{\sqrt{1 + A^2 \sin^2 \Theta}} + \tan^{-1} \frac{B - A \cos \Theta}{\sqrt{1 + A^2 \sin^2 \Theta}} \right] \\
 &+ \cos \Theta \int_0^B \sqrt{1 + \xi^2 \sin^2 \Theta} \\
 &\quad \left( \tan^{-1} \frac{A - \xi \cos \Theta}{\sqrt{1 + \xi^2 \sin^2 \Theta}} + \tan^{-1} \frac{\xi \cos \Theta}{\sqrt{1 + \xi^2 \sin^2 \Theta}} \right) d\xi
 \end{aligned}$$

We will notice that this configuration has the particularity to have facets having a common edge. Mathematically this means that the function to integrate becomes singular (since it involves the distance between the points of the edges). However, the integral of this singular function remains bounded (the energy remains finite).

Results are :

Angle $\theta$	Analytique	SYRTHES
30	0.619028	0.61902831
60	0.370905	0.37090532
90	0.200044	0.20004377
120	0.086615	0.08661500
150	0.021346	0.02134532
180	0.	0.00000002

### 10.1.3 View factors in a cylinder

The following is the surfacic mesh of the cylinder that was used to calculate the view factors (1064 faces).

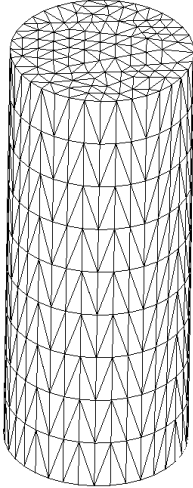


Figure 10.3: Mesh for view factors calculation

We remind you that we have to check :  $\sum_{j=1}^N F_{ij} = 1$  (this relationship comes from the conservation of energy).

The following figure shows the values of the of the sum of the view factors for each of the faces of the mesh. We can notice that the maximum error on the sum is of the order of  $10^{-6}$ .

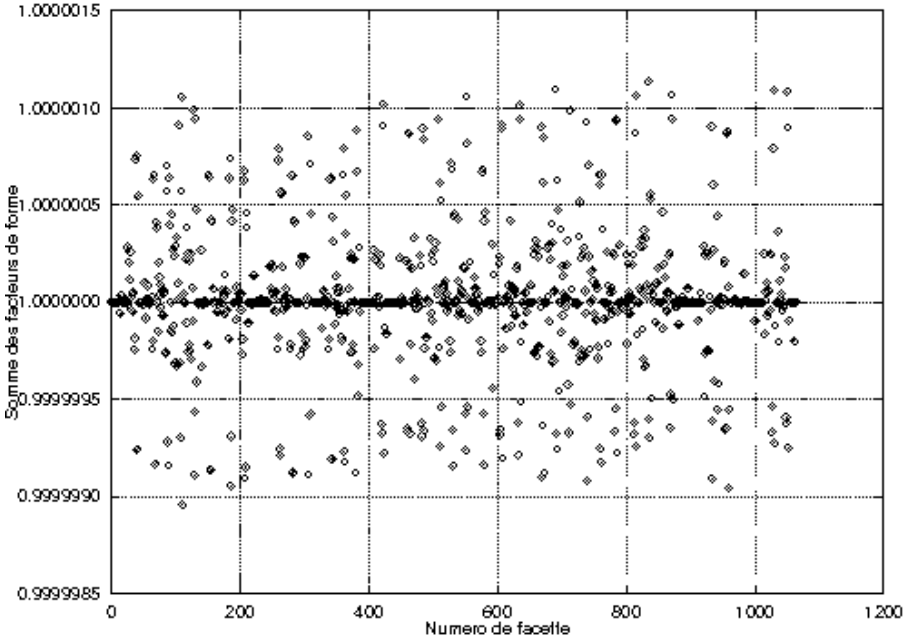


Figure 10.4: Sum of the view factors

Note :  
*Strictly speaking, this test ensures that the energy is well conserved but not to assert that each of the view factors is calculated as precisely as possible.*

## 10.2 Axisymmetric view factors

### 10.2.1 Case of 2 rings on a cylinder

We wish to calculate the view factor between two rings defined on a cylinder of radius  $r$ . The calculation is done in axisymmetric. For SYRTHES, the mesh required for the calculation is reduced to two vertical segments. The case is presented on the figure 10.5 :

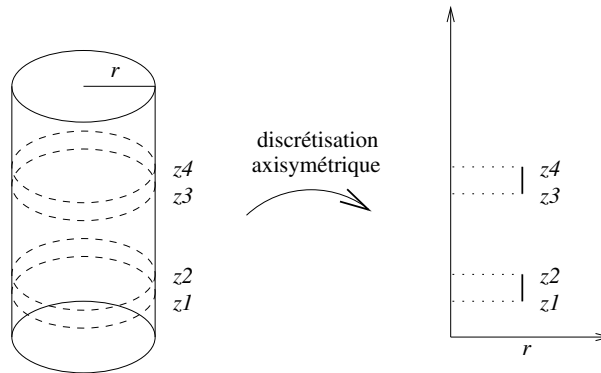


Figure 10.5: 2 rings on a cylinder - axisymmetric calculation

Surface 1 is defined by the ring  $z_1 - z_2$  and surface 2 by the ring  $z_3 - z_4$ . The expression of the view factor is given by

$$F_{12} = \frac{1}{4r(z_2 - z_1)} [f(z_2 - z_3) - f(z_2 - z_4) + f(z_1 - z_4) - f(z_1 - z_3)]$$

avec

$$f(x) = x^2 - |x|\sqrt{x^2 + 4r^2} + 2r|x|$$

For such a configuration, all the points of the first ring see all the points of the second ring. The case has been studied for various configurations by varying the thickness of the upper ring and the distance between the two rings.

The results are presented in the table below. We will note a very good precision of the results provided by SYRTHES.

r	z1	z2	z3	z4	Analytical values	Numerical calculation
1	0	0.1	1.	1.1	0.0187129268378	0.018712926838
1	0	0.1	0.5	0.6	0.0321822739118	0.032182273911
1	0	0.1	0.11	0.21	0.0458896098695	0.045889609869
1	0	0.1	0.1	0.2	0.0462616576130	0.046261657613
1	0	0.1	0.2	0.7	0.1782713873497	0.178271362840

### 10.2.2 Case of 2 rings on a cone

We wish to calculate the form factor between two rings defined on a cone. The latter is characterized by the radius of its base  $r$  and its opening  $\psi$ . The calculation is done in axisymmetric. For SYRTHES, the mesh required for the calculation is reduced to two inclined segments.

The case is presented on the figure 10.6 :

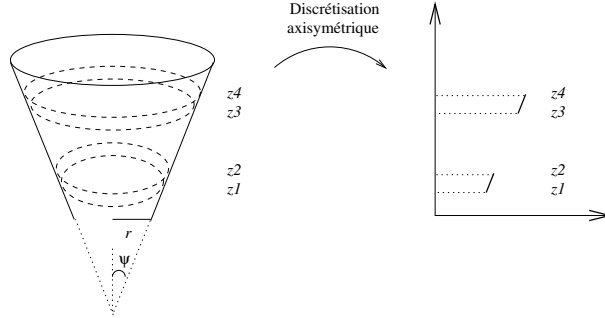


Figure 10.6: 2 rings on a cone - axisymmetric calculation

Surface 1 is defined by the ring  $z_1 - z_2$  and surface 2 by the ring  $z_3 - z_4$ .

The expression of the view factor is given by

$$F_{12} = \frac{\frac{1}{2} \sin \psi}{2r(z_2 - z_1) + \frac{z_2^2 - z_1^2}{\tan \psi}} \times [2(z_2 - z_1)(z_4 - z_3) + f(z_2, z_4) - f(z_1, z_4) + f(z_1, z_3) - f(z_2, z_3)]$$

with

$$f(x, y) = \frac{\sqrt{\left[ (x - y)^2 + \left( r + \frac{x}{\tan \psi} \right)^2 + \left( r + \frac{y}{\tan \psi} \right)^2 \right]^2 - \left[ 2 \left( r + \frac{x}{\tan \psi} \right) \left( r + \frac{y}{\tan \psi} \right) \right]^2}}{2 \left( r + \frac{x}{\tan \psi} \right) \left( r + \frac{y}{\tan \psi} \right)}$$

The calculation was made for two different opening angles and in each case for two different ring thicknesses.

The results are presented in the table below. We will note a very good accuracy of the results provided by SYRTHES.

$r$	$\psi$	$z1$	$z2$	$z3$	$z4$	Analytical values	Numerical calculation
0.5	$\pi/6$	0.	0.1	0.5	0.6	0.0145100568276	0.014510056830
0.5	$\pi/6$	0.	0.1	0.2	0.25	0.0139078991326	0.013907899019
0.5	$\pi/4$	0.	0.1	0.5	0.6	0.0260748111926	0.026074811215
0.5	$\pi/4$	0.	0.1	0.2	0.25	0.0229771224013	0.022977122422

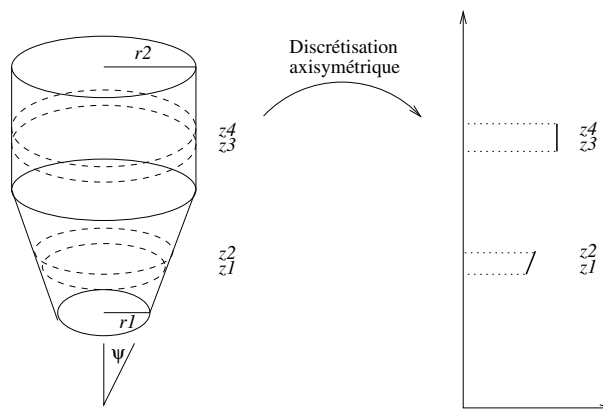


Figure 10.7: Rings on a cone and a cylinder - Axisymmetric calculation

### 10.2.3 Case of a ring on a cone, the other on a cylinder

We wish to calculate the view factor between two rings, the first one being defined on a truncated cone, the second on a cylinder. The truncated cone is characterized by the radius of its base  $r_1$  and its opening  $\psi$ , the cylinder has a radius  $r_2$ . The calculation is done in axisymmetric. For SYRTHES, the mesh required for the calculation is reduced to two segments, one vertical, the other inclined.

The case is presented on the figure 10.7 :

View factor is given by

$$F_{12} = \frac{\frac{1}{2} \sin \psi}{2r_1(z_2 - z_1) + \frac{z_2^2 - z_1^2}{\tan \psi}} \times [2(z_2 - z_1)(z_4 - z_3) + f(z_3, z_1) - f(z_3, z_2) + f(z_4, z_2) - f(z_4, z_1)]$$

avec

$$f(x, y) = \sqrt{\left[ (x - y)^2 + r_2^2 + \left( r_1 + \frac{y}{\tan \psi} \right)^2 \right]^2 - \left[ 2r_2 \left( r_1 + \frac{y}{\tan \psi} \right) \right]^2}$$

The calculation was made for two different opening angles and in each case for two different ring thicknesses.

The results are presented in the table below. We will note a very good accuracy of the results provided by SYRTHES.

$r_1$	$r_2$	$\psi$	$z_1$	$z_2$	$z_3$	$z_4$	Analytical values	Numerical calculation
0.5	1.	$\pi/6$	0.	0.1	0.5	0.6	0.0655544734077	0.065554508966
0.5	1.	$\pi/4$	0.	0.1	0.5	0.6	0.0535358509414	0.053535849698
0.5	1.	$\pi/6$	0.	0.1	0.12	0.7	0.2821714144798	0.281463904352
0.5	1.	$\pi/4$	0.	0.1	0.12	0.7	0.1838728520392	0.183610892562

### 10.2.4 Case of 2 rings face to face

We wish to calculate the view factor between two rings facing each other. The rings are characterized by their radius. The calculation is done in axisymmetric. For SYRTHES, the mesh required for the calculation is reduced to two horizontal segments. The case is presented on the figure : 10.8 :

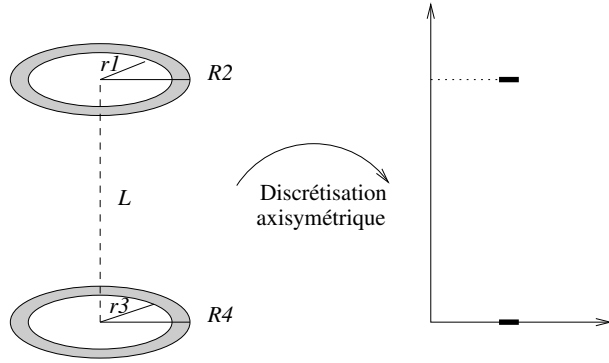


Figure 10.8: Anneaux en vis-a-vis - calcul en axisymétrique

$$F_{12} = \frac{1}{2} \left[ \frac{R_4^2 - r_3^2}{r_1^2} - \sqrt{\left(1 + \frac{R_4^2 + L^2}{r_1^2}\right)^2 - 4\frac{R_4^2}{r_1^2}} + \sqrt{\left(1 + \frac{r_3^2 + L^2}{r_1^2}\right)^2 - 4\frac{r_3^2}{r_1^2}} \right]$$

The calculation has been done for several values of the distance  $L$  between the two rings. The results are presented in the table below.

$r1$	$R2$	$r3$	$R4$	$L$	Analytical values	Numerical calculation
0.5	0.6	0.5	0.6	1.	0.0535424552602	0.053542455350
0.5	0.6	0.5	0.6	0.5	0.1055306803864	0.105530689990
0.5	0.6	0.5	0.6	0.1	0.4158876592597	0.415941427592

We notice, as in the case of two planes facing each other, that the numerical estimation of the view factors is better when the distance between the 2 disks is high. The reason is the same.

**10.2.5 Hidden faces : disk perpendicular to a cylinder**

We are now interested in the axisymmetric configurations with shading calculations.

The case is presented below. It is the calculation of the view factor between a disk  $D$  and a cylinder  $C$ .

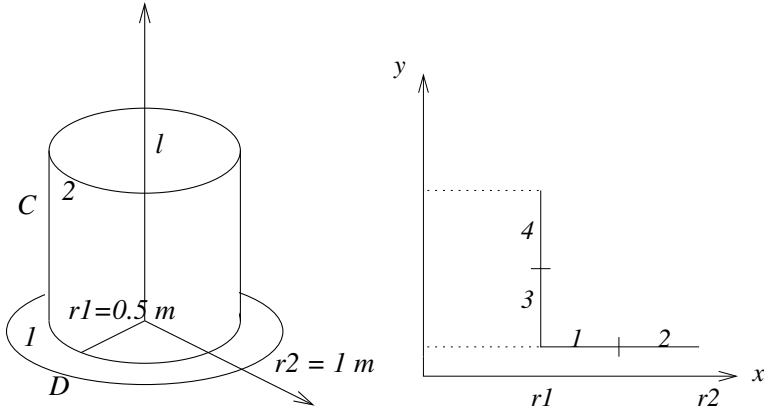


Figure 10.9: Case of a disk perpendicular to a cylinder

We define

$$R = \frac{r_2}{r_1} \quad L = \frac{l}{r_1}$$

Then, we have

$$\begin{aligned}
 F_{12} = & \frac{1}{\pi(1 - R^2)} \left[ (1 - R^2) \tan^{-1} \sqrt{\frac{1 + R}{1 - R}} \right. \\
 & - \sqrt{(1 + R^2 + L^2)^2 - 4R^2} \tan^{-1} \sqrt{\frac{(1 + R^2 + L^2 + 2R)(1 - R)}{(1 + R^2 + L^2 - 2R)(1 + R)}} \\
 & \left. + \frac{1}{2} L^2 \cos^{-1} R + 2RL \tan^{-1} \frac{\sqrt{1 - R^2}}{L} \right].
 \end{aligned}$$

Based on this test case, we will consider 4 faces. The first two are on the disk  $D$  (faces 1 and 2), the 2 following ones on the cylinder  $C$  (faces 3 and 4).

These tests involve the calculation of the hidden surfaces. When a shading is detected, it is possible to ask the code for an automatic re-cutting of the faces in order to obtain locally a better discretization of the geometry. In the case of segments, the first resharpening leads to consider 2 sub-segments. When we ask for 2 reslicings, we will finally consider the 4 sub-segments which constitute each segment.

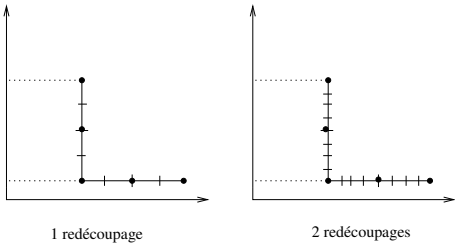


Figure 10.10: Re-cutting of faces

The table below shows the values of the surface multiplied by the view factor for a couple of faces. We also present results with 1 and 2 re-cuts of the faces.

Surf x view factor	$S_4F_{41}$	$S_3F_{32}$
Analytique	0.0827264975	0.2155427154
0 redecoupage	0.08259126	0.21264747
1 redecoupage	0.08267165	0.21389134
2 redecoupages	0.08270403	0.21463669

Note *It can be noted that the view factor  $S_4F_{41}$  is better estimated than  $S_3F_{32}$ . It is possible that the angular discretization is more important for more distant faces.*

### 10.2.6 Hidden faces : two concentric cylinders

The case is shown in the following figure

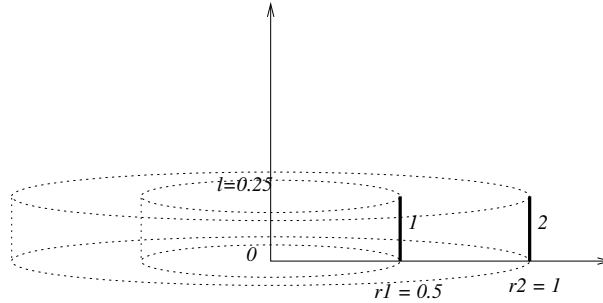


Figure 10.11: Case of two concentric cylinders

We define

$$R = \frac{r_2}{r_1}$$

$$L = \frac{l}{r_1}$$

Then, we have

$$F_{12} = \frac{1}{R} - \frac{1}{\pi R} \left\{ \cos^{-1} \frac{B}{A} - \frac{1}{2L} \left[ \sqrt{(A+2)^2 - 4R^2} \cos^{-1} \frac{B}{RA} + B \sin^{-1} \frac{1}{R} \frac{\pi A}{2} \right] \right\}$$

The table below shows the values of the surface multiplied by the view factor of the two faces. As in the case 10.2.5, we also present the results with 1 and 2 re-cutting of the faces.

Surf x View factor	$S_1 F_{12}$
Analytique	0.21094110
0 recoupage	0.21094158
1 recoupage	0.21094158
2 recoupages	0.21094158

Note :

*We notice that in this particular case, the fact of re-cutting does not lead to an improvement of the result. The explanation lies in the fact that, on this example, the angular position corresponding to the masking caused by the face 1 (inner cylinder) corresponds to the same limit angle whether the segments are re-cut or not. This would no longer be true if there were an intermediate obstacle.*

A similar case has been tested by bringing the 2 cylinders closer.

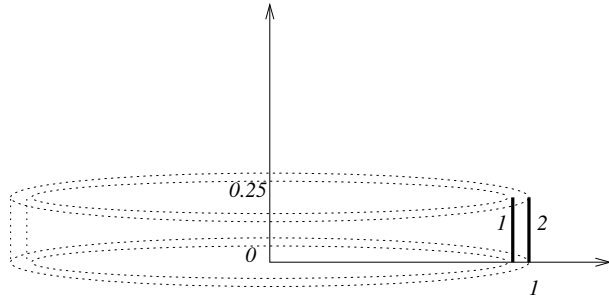


Figure 10.12: Case of two concentric cylinders at short distance

Surf x view factor	$S_1 F_{12}$
Analytique	1.2384039767
0 redécoupage	1.23842909
1 redécoupage	1.23842908

Note :

*As in the previous case, the re-cutting does not bring any improvement and the same remark concerning the limit angles applies.*

### 10.2.7 Hidden faces : cone and disk

We consider 2 faces on a 45° cone and 2 others on a disk. Le cas est presente sur la figure suivante

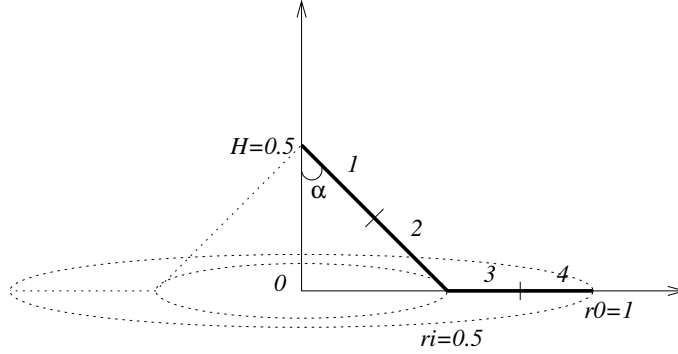


Figure 10.13: Faces on a cone and a disk

Analytical formulas exist, but are becoming very complex.

We define  $R_i = r_i/r_o$ , and the auxiliary terms

$$A = \sqrt{H^2 + (1 + H \tan \alpha + R_i)^2}$$

$$B = \sqrt{H^2 + (1 - H \tan \alpha - R_i)^2}$$

$$C = \sqrt{1 - R_i^2}$$

$$D = \sqrt{1 + R_i^2}$$

$$E = \cos^2 \alpha (1 - R_i^2)$$

We have

$$F_{41} = \frac{1}{\pi(1 - R_i^2)} \left\{ -AB \tan^{-1} \frac{AB}{CD} + C^2 D^2 \tan^{-1} \frac{D}{C} \right. \\ \left. + \frac{\sin \alpha}{\cos^2 \alpha} \left[ \left( H^2 + \frac{2HR_i}{\tan \alpha} \right) \tan^{-1} \frac{\sqrt{E}}{H} + E \tan^{-1} \frac{H}{\sqrt{E}} \right] \right. \\ \left. + \left( \frac{H^2}{2 \cos^2 \alpha} + HR_i \tan \alpha \right) \cos^{-1} R_i \right\}$$

The table below shows the values of the area multiplied by the view factor for the pair of 4-1 faces. As in the case 10.2.5, we present also the results with 1 and 2 re-cutting of the facettes.

Surf x view factor	$S_4 F_{41}$
Analytique	0.00530000448
0 redécoupage	0.00527607
1 redécoupage	0.00528986
2 redécoupages	0.00529548

Note :

*Unlike the previous configurations, we note in this case an improvement of the view factor with the number of recuts. This is due to the fact that with a recutting, each sub-segment is better estimated.*

## 10.3 Summary of view factor validation

On a vu dans les paragraphes precedents que les facteurs de forme (quantite purement geometrique) sont estimes de facon rigoureuse dans SYRTHES, au moins dans le cas de configurations simples pour lesquelles des solutions analytiques existent.

Cela ne signifie pas que toutes les situations rencontrees dans les cas industriels seront calculees avec ce niveau de precision. En effet, les effets d'ombrage sont particulierement difficiles a prendre en compte et l'on manque de configurations de reference.

C'est pourquoi les auteurs insistent sur l'importance que peut avoir la realisation du maillage de rayonnement sur la qualite des resultats. Il convient en particulier d'utiliser des elements dont la taille est en rapport avec le probleme physique que l'on souhaite traiter (pas trop grands dans les zones a forts gradients, dans les zones d'ombrages, etc...). En effet, on rappelle que, d'une part, la temperature est supposee constante par facette (methode de radiosite) et que d'autre part, des elements de taille non adaptee pourraient induire des erreurs sur l'influence des facette oculutrices.

Nous venons egalement de montrer que le redécoupage automatique des facettes pouvait ameliorer le calcul des facteurs de forme. Il faut toutefois garder a l'esprit qu'il reste preferable d'utiliser un maillage adapte (suffisamment fin aux endroits delicats). En effet, si le redécoupage permet d'augmenter la precision des facteurs de forme, la temperature n'en reste pas moins constante par facette. Par ailleurs, le redécoupage est une option qui entraine un surcout important : un facteur 4 pour 1 redécoupage, un facteur 16 pour 2 redécoupages, etc... Meme si ces donnees geometriques ne sont calculees qu'une fois par calcul, le cout CPU peut etre non negligeable. Les procedures de calcul utilisees devraient cependant limiter le cout CPU a des valeurs raisonnables.

We have seen in the previous paragraphs that the view factors (purely geometrical quantity) are rigorously estimated in SYRTHES, at least in the case of simple configurations for which analytical solutions exist. This does not mean that all situations encountered in industrial cases will be computed with this level of accuracy. Indeed, the shading effects are particularly difficult to take into account and there is a lack of reference configurations.

This is why the authors insist on the importance radiation mesh building phase : quality of the radiation mesh induces directly the quality of the results. In particular, it is advisable to use elements whose size is related to the physical problem (not too big in the zones with strong gradients, in the shaded areas, etc...). Indeed, we recall that, firstly, the temperature is supposed to be constant per face (radiosity method) and secondly, that elements with a non adapted size could induce errors on occulting faces.

We have also just shown that the automatic facet resizing could improve the view factors. However, we have to keep in mind that it is still better to use an adapted mesh (locally fine enough). Indeed, if the reslicing allows to increase the accuracy of the view factors, the temperature remains constant per facet. Moreover, reslicing is an option that involves a significant additional cost : a factor of 4 for 1 recut, a factor of 16 for 2 recuts, etc... Even if these geometrical data are calculated only once per calculation, the CPU cost can be non negligible. The calculation procedures used should however limit the CPU cost to reasonable values.

## Chapter 11

# Solver validation

The previous test cases have allowed us to appreciate the quality of the view factors. Then, we have to validate the solver for the resolution of the radiation system.

We consider a cylinder of height  $L$  and radius  $R$ . The temperature of the ambient medium ( $T_e$ ) is fixed at 0, the temperature of the cylinder and its base is fixed at  $T_w$ , we calculate the radiative radiative flux  $Q$  passing through the upper face of the cylinder.

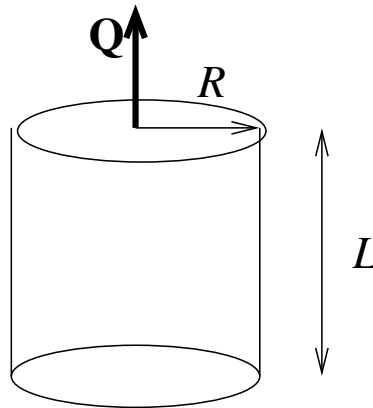


Figure 11.1: Calculation part

From these quantities, we can build an equivalent emissivity:

$$\varepsilon = \frac{Q}{\pi R^2 \sigma (T_w^4 - T_e^4)}$$

The test case is realized for several values of the ratio  $L/R$ .

The meshes used for the different ratios of  $L/R$  are following :

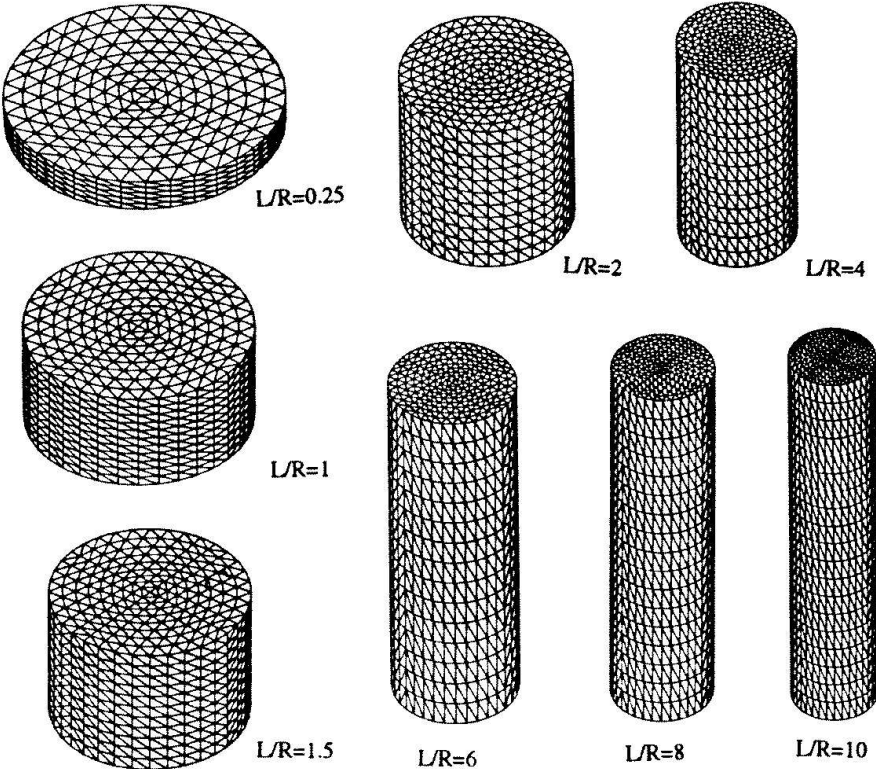
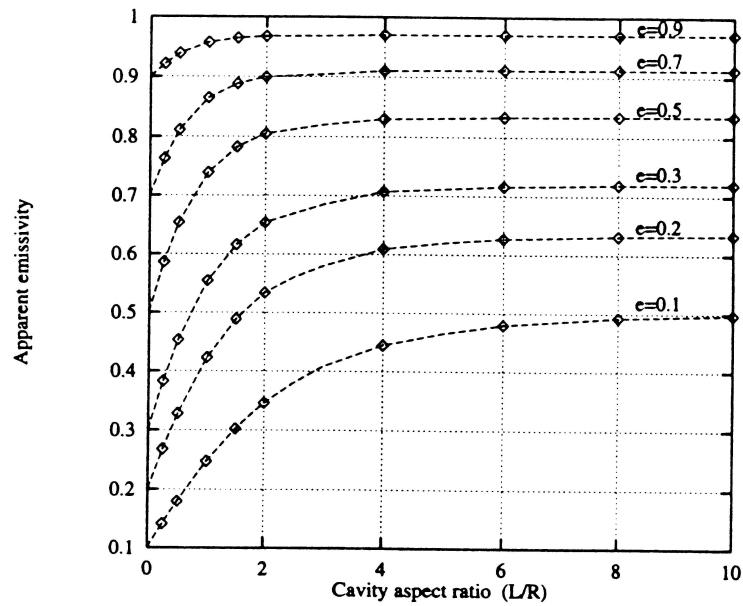


Figure 11.2: the meshes used

The section of all cylinders is identically discretized. It consists of 324 elements. The number of vertical sections is shown in the following table

L/R	0.25	1	1.5	2	4	6	8	10
Sections	6	12	12	12	14	16	18	20

Then we plot the value of the flux for different ratios  $L/R$  and for different values of the emissivity  $\varepsilon$ . (the diamonds indicate the analytical values). The analytical values are taken from the literature.



The good agreement between the numerical results and the reference values show :

- that the view factors have been evaluated correctly, which is not surprising considering the tests performed on the elementary configurations and on the cylinder presented in paragraph ??,
- that the radiosities are evaluated correctly. This indicates a rigorous resolution of the radiative system.

## Chapter 12

# CHANNEL\_RAD

**Characteristics :** Stationnary 2D cartesian, coupling conduction/radiation.

**Objectives :** Validation of radiative calculation in 2D cartesian and validation of coupling conduction/radiation.

### 12.1 Test case description

#### 12.1.1 Geometry

Consider a channel of infinite length in order to be able to assume that thermal transfers are 1D inside a slice. This allows to compare calculation results to a analytical solution.

In practice, we define a channel one meter long and 3 cm wide. The walls thickness is 1 cm.



Figure 12.1: Solid domain

#### 12.1.2 Physical conditions

The solid is related to steel having following physical characteristics :

- conductivity  $k = 25 W/mK$
- density  $\rho = 7700kg/m^3$
- specific heat  $C_p = 460J/kgK$

Lower wall's emissivity is fixed to 0.5 and the one of the upper wall at 0.8.

#### 12.1.3 Initial conditions, boundary conditions

Initially (at  $t = 0$ ), the solid is at  $0^\circ C$ . We impose on the lower wall a temperature  $T_1 = 1000^\circ C$  and on the upper wall a temperature  $T_4 = 0^\circ C$ .

## 12.2 Analytical solution

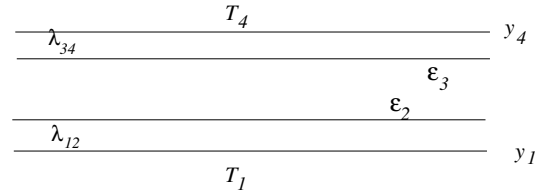


Figure 12.2: 2 parallel plates

In the case of 2 parallel plates, the temperature profile in thickness is given by  $T(y) = \varphi \frac{y-y_1}{\lambda_{12}} + T_1$  in the lower part and  $T(y) = \varphi \frac{y-y_4}{\lambda_{34}} + T_4$  in the upper part. where  $\varphi$  is a solution of the equation

$$\varphi - \sigma \frac{\varepsilon_2 \varepsilon_3}{\varepsilon_2 + \varepsilon_3 - \varepsilon_2 \varepsilon_3} \left[ \left( -\frac{\lambda_{34}}{d_{34}} \varphi + T_4 \right)^4 - \left( \frac{\lambda_{12}}{d_{12}} \varphi + T_1 \right)^4 \right] = 0$$

In the present case we have following datas :

- $\lambda_{12} = \lambda_{34} = 25 \text{ W/mK}$
- $\varepsilon_2 = 0.5, \varepsilon_3 = 0.8$
- $T_1 = 1000^\circ\text{C}, T_4 = 0^\circ\text{C}$

The previous equation's solution is then  $\varphi = -61070.27839 \text{ W/m}^2$

## 12.3 Calculation description

### 12.3.1 Meshes

The mesh is realised in 2 dimension.

Conduction mesh counts :

- 1782 nodes,
- 784 triangles.

Regarding radiation, the mesh counts 102 facets.

It is closed to both ends by an imposed temperature condition at  $0^\circ\text{C}$ . We assume the domain long enough for this condition has no influence on the channel center where it perfoms comparisons.

## 12.4 Presentation of results

A calculation was performed with a time step equal to 0.3 seconds, which provides a good precision of the transient calculation (although only stationary solution could be compared to analytical values, lack of formula discribing transient<sup>1</sup>).

Convergence is reached after 75 physical seconds representing 250 time steps.

<sup>1</sup>Any proposal of an analytical unstationnary solution for this configuration would be welcome.

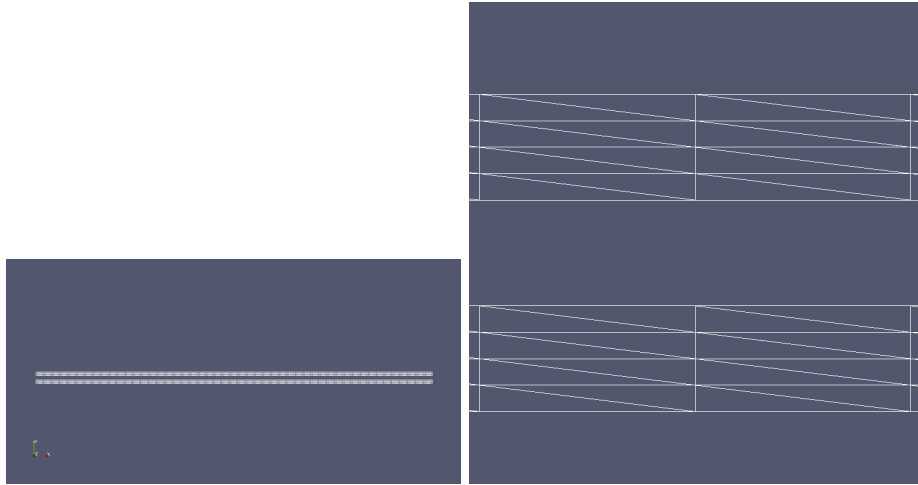


Figure 12.3: Mesh for conduction

### 12.4.1 Comparison calculation results / analytical value

Comparisons between calculated values and analytical values are made in the middle of the channel in  $y=0.51$ .

We can note a very good adequacy between theoretical profiles and values given by SYRTHES.

We can compare temperature values in  $y = 0.01$  et  $y = 0.02$  (which correspond to inner faces).

Ordinate	analytical T	T SYRTHES
0.01	9.755718886e+02	9.755615295e+02
0.02	2.44281136e+01	2.441899313e+01

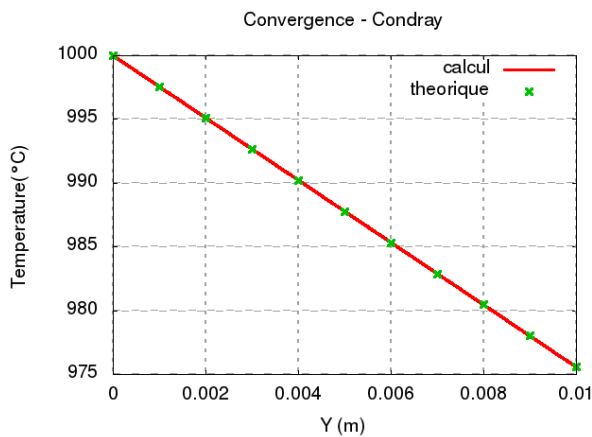
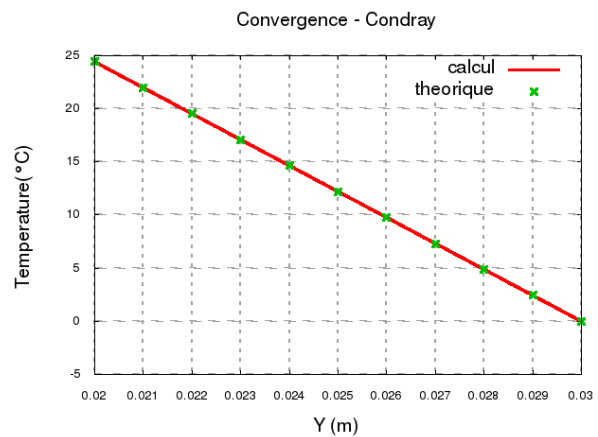


Figure 12.4: Lower wall



Upper wall

### 12.4.2 Thermal field inside plates

The thermal field at convergence is presented on the figure [12.5](#).

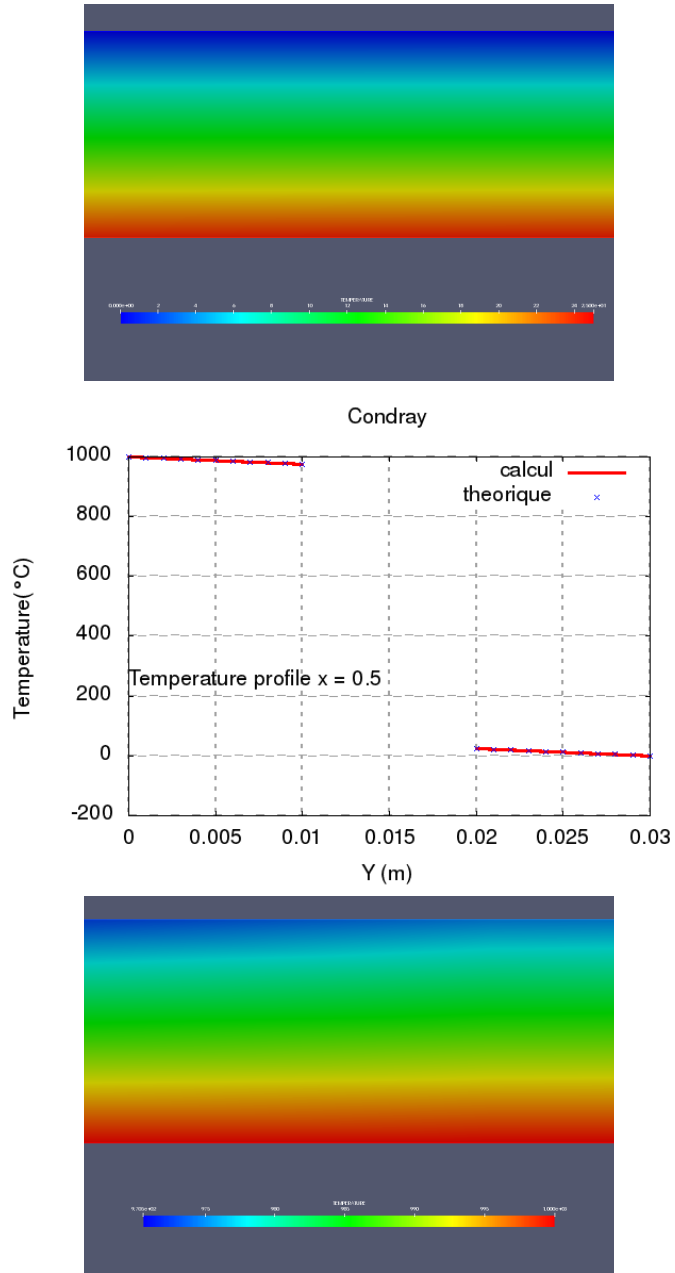


Figure 12.5: Thermal field at convergence

### 12.4.3 Study of calculation's convergence

The figure 12.6 show temperature evolution in 4 points all located in  $x = 0.51$  (center of the channel) and respectively at 0.0025 (A), 0.0075 (B), 0.0225 (C), 0.0275(D).

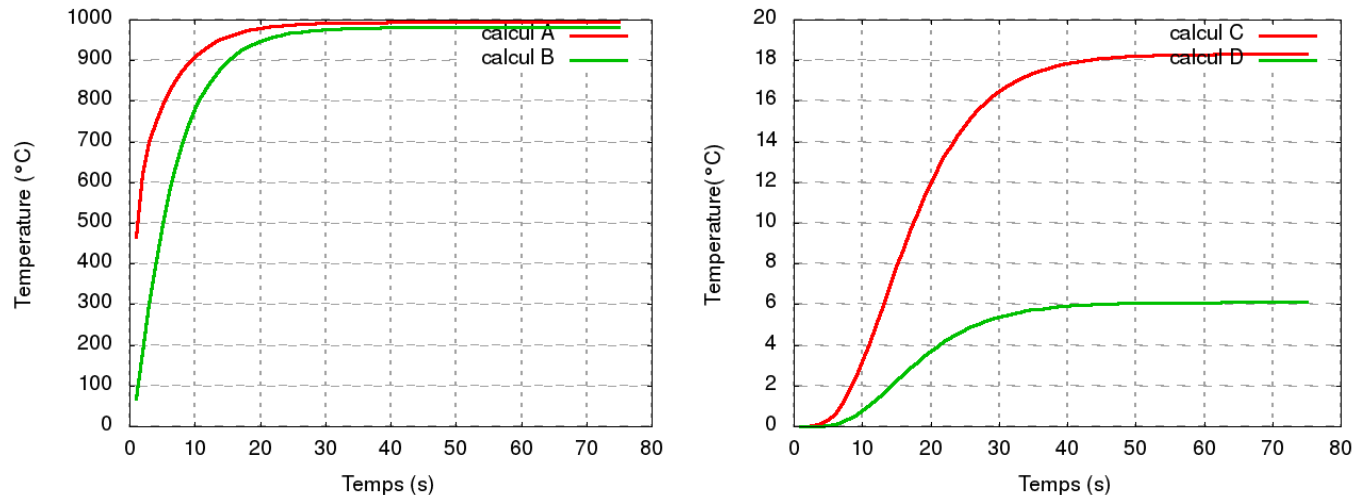


Figure 12.6: Lower wall

Upper wall

## 12.5 Synthesis

Results obtained with SYRTHES on this case are satisfactory.

We could test several aspects :

- meshes reading fo conduction and radiation,
- calculation of view factor in 2D cartesian (faces entirely visible),
- radiative boundary condition and imposed temperature,
- resolution of radiative system,
- resolution of conductive system,
- interpolation between conduction meshes and radiation,
- coupling in conduction and radiation (realised, it reminds, by linearization of radiative exchanges, and treated explicitly).

## Chapter 13

# CYLINDERS\_2D\_RAD

**Characteristics :** Steady state, 2D, cartesian symmetry, coupling conduction/radiation.

**Objectives :** Validation of radiative calculation in 2D cartesian with shading calculation and consideration of symmetry. Validation of coupling conduction/radiation.

### 13.1 Test case description

#### 13.1.1 Geometry

Consider two cylinders concentrically nested. Cylinders are considered infinite in length and can be modeled in 2D.

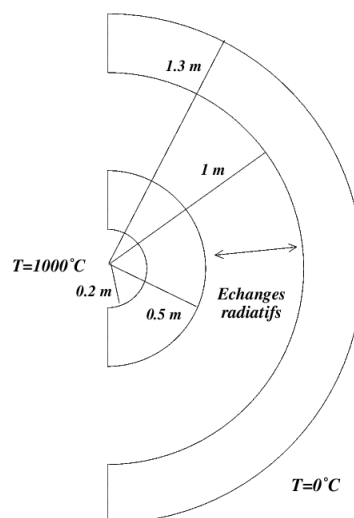


Figure 13.1: Solid domain

#### 13.1.2 Physical conditions

The solid is related to steel having following physical characteristics :

- conductivity  $k = 25 \text{ W/mK}$
- density  $\rho = 7700 \text{ kg/m}^3$
- specific heat  $C_p = 460 \text{ J/kgK}$

### 13.1.3 Initial conditions, boundary conditions

Initially (at  $t = 0$ ), the solid is at  $0^\circ C$ . We impose on the inner surface of the inner sphere a temperature  $T_1 = 1000^\circ C$  and on outer surface of the outer sphere a temperature  $T_4 = 0^\circ C$ .

## 13.2 Analytical solution

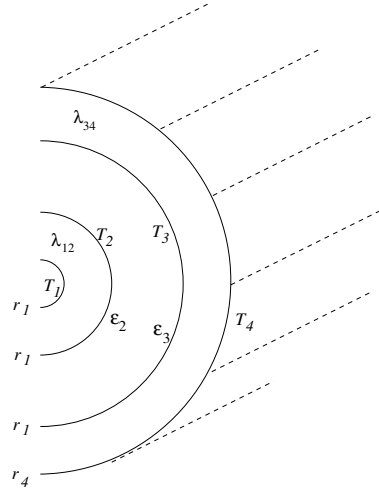


Figure 13.2: 2 infinite concentric cylinder

In the case of 2 concentric cylinder, the flux  $\varphi$  which passes through the surfaces is a solution of the equation

$$\varphi \left( \frac{1}{\varepsilon_2} + \frac{r_2}{r_3} \left( \frac{1}{\varepsilon_3} - 1 \right) \right) - s_2 \sigma \left[ \left( T_1 + \frac{\varphi r_1 \log \frac{r_1}{r_2}}{s_1 \lambda_{12}} \right)^4 - \left( T_4 - \frac{\varphi r_4 \log \frac{r_3}{r_4}}{s_4 \lambda_{34}} \right)^4 \right] = 0$$

In present case we have following data :

- conductivities  $\lambda_{12} = \lambda_{34} = 25 \text{ W/mK}$
- emissivities  $\varepsilon_2 = 0.5, \varepsilon_3 = 0.8$
- edge temperatures  $T_1 = 1000^\circ C, T_4 = 0^\circ C$
- radii  $r_1 = 0.2, r_2 = 0.5, r_3 = 1., r_4 = 1.3$
- surfaces  $s_1 = 2\pi r_1, s_2 = 2\pi r_2, s_3 = 2\pi r_3, s_4 = 2\pi r_4,$

Solution of previous equation is then  $\varphi = 59706.82602 \text{ W/m}^2$  Then we obtain inner walls temperatures

$$T_2 = T_1 + \varphi \frac{\log \frac{r_1}{r_2}}{2\pi \lambda_{12}} = 651.712890^\circ C$$

$$T_3 = T_4 - \varphi \frac{\log \frac{r_3}{r_4}}{2\pi \lambda_{34}} = 99.7260894^\circ C$$

Temperature profile in a radius of the inner cylinder is given by

$$T(r) = T_1 + \frac{T_1 - T_2}{\log \frac{r_1}{r_2}} \log \frac{r}{r_1}$$

and temperature profile in a radius of the outer cylinder by

$$T(r) = T_4 + \frac{T_3 - T_4}{\log \frac{r_3}{r_4}} \log \frac{r}{r_4}$$

We note of course, that at steady state, solution doesn't depend on density and heat capacity any more. These terms change only the thermal inertia of the solid part and occur only during transient.

## 13.3 Calculation description

### 13.3.1 Meshes

In so far as cylinders are supposed of infinite length, we suppose the phenomena in two dimensions and the mesh is then built in 2D.

The mesh has :

- 1 482 nodes with 369 vertex nodes,
- 672 triangles.

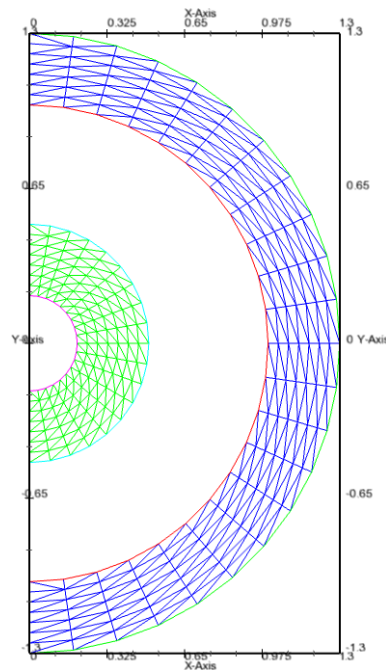


Figure 13.3: Conduction mesh

Note that we use here the symmetry properties which exist in the problem. For conduction, this lead only to impose a null flux. On the other hand, for radiation, it requires that the method can take into account rigorously interaction between the facets of both sides of the plane of symmetry.

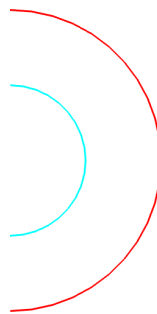


Figure 13.4: Mesh for radiation

Regarding radiation, the mesh is formed by two circular arcs of radius respectively 0.5 m and 1 m. It counts 56 facets.

### 13.4 Presentation of results

We have performed calculation with a time step equal to 200 seconds. Convergence has been reached after about 100 000 physical seconds (about 28 hours), with 500 time steps.

#### 13.4.1 Temperature field inside cylinders

We present here the temperature field at convergence.

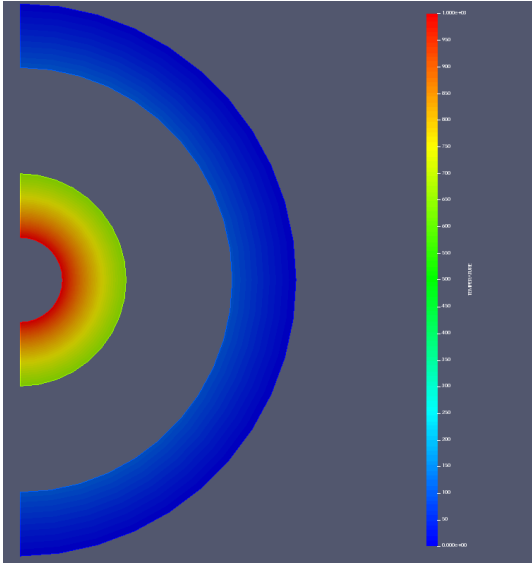


Figure 13.5: Temperature field at convergence

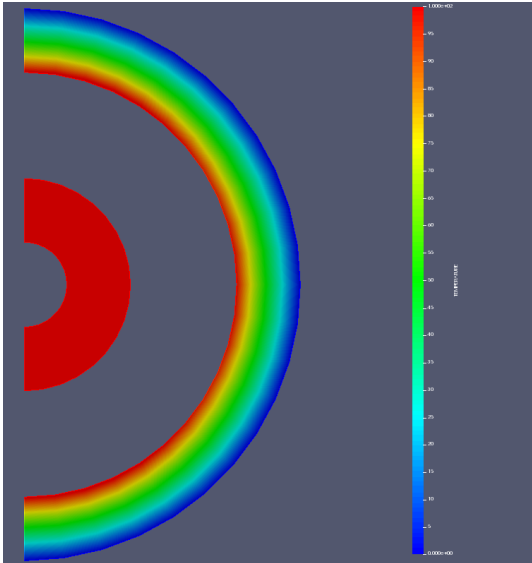


Figure 13.6: Temperature profile at convergence

The figure 13.7 presents temperature domain at convergence but with a temperature which allows to visualize warming of outer cylinder. We also present the temperature profile at  $y=0$ .

Note that despite the use of a plane of symmetry, the field obtained complies with the axisymmetric nature of the problem.

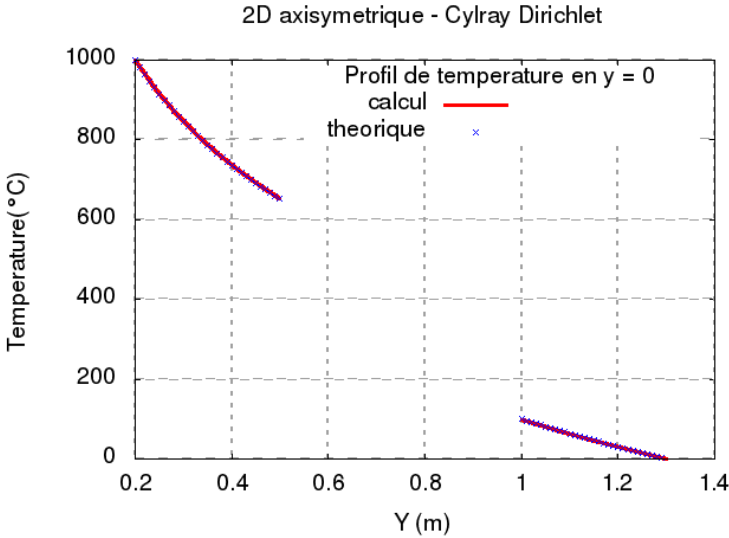


Figure 13.7: Temperature profile at convergence

### 13.4.2 Comparison calculation results / analytical values

Comparisons between calculated values of temperature and analytical values are made along a radius of cylinders.

We note, on figure 13.8, a very good agreement between the theoretical profiles and values given by SYRTHES.

#### Comparisons between analytical profiles and calculated ones

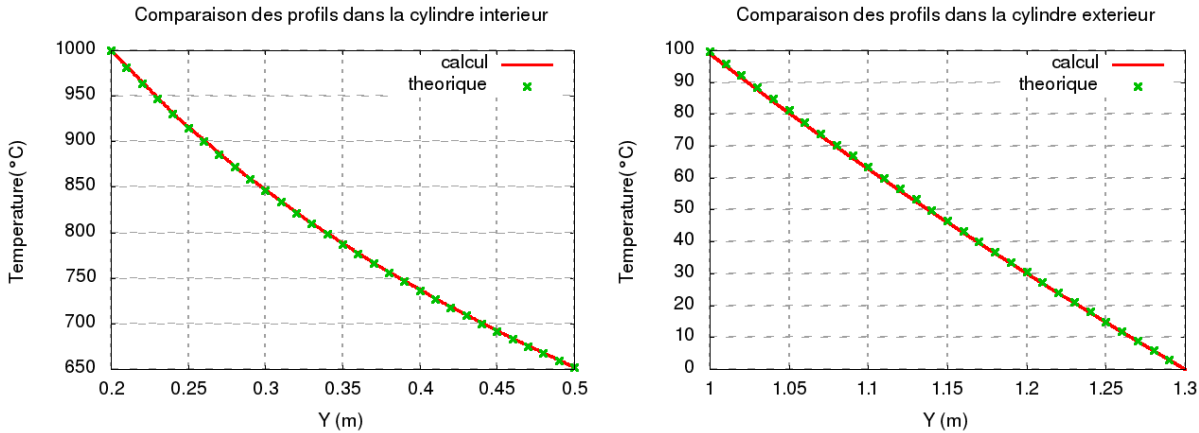


Figure 13.8: Inner cylinder

outer cylinder

In the table below, we compare temperature values in  $r = 0.5$  and  $r = 1$

Ordinate	analytical T	T SYRTHES
0.5	6.51712890e+02	6.522676381e+02
1.	9.97260894e+01	9.885848739e+01

### 13.4.3 Study of calculation's convergence

The following figure shows temperature's evolution in 6 points along  $y=0$  :  $x=0.3$  (A),  $x=0.4$  (B),  $x=0.5$  (C),  $x=1.$  (D),  $x=1.1$  (E),  $x=1.2$  (F).

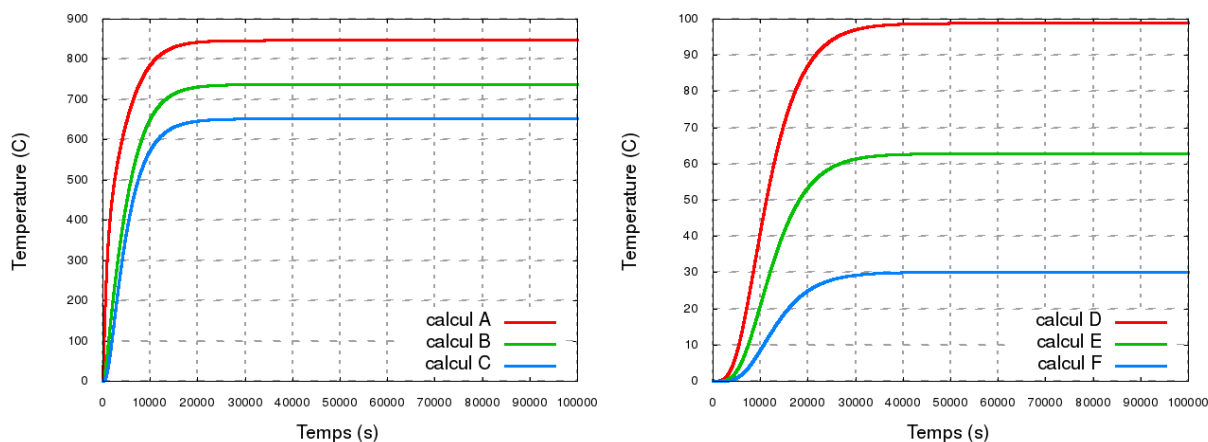


Figure 13.9: Inner cylinder

Outer cylinder

The calculation was conducted on a physical time quite long because very small changes in temperature could still be observed after more 70000 physical seconds.

Remarks :

- Like in the previous case, it would be very useful to have unstationnary analytical solutions for this type of configuration. If they exist, they are probably very complex.
- Note that the temperature field obtained complies with the polar nature of the problem, even if a symmetry condition has been used.

## 13.5 Synthesis

Results obtained with SYRTHES on this case are satisfactory.

This configuration has allowed to check particularly several aspects :

- calculation of view factor in 2D cartesian,
- calculation of shadowing,
- taking into account of a symmetry. It confirms the harsh treatment of symmetries in radiation,
- calculation of elementary matrices in 2D cartesian,
- coupling in conduction and radiation with a circular interface.

Note that if this configuration appears as if possessing a 1D solution in cylindrical system, it is 2D when it is used in cartesian coordinates as this is the case in SYRTHES.

## Chapter 14

# SPHERE\_RAD

**Characteristics :** 3D (here represented by a 2D axisymmetric discretization), steady state, coupling conduction/radiation.

**Objectives :** Validation of radiative calculation in axisymmetric and validation of coupling conduction/radiation.

### 14.1 Test case description

#### 14.1.1 Geometry

We consider 2 nested hollow spheres :

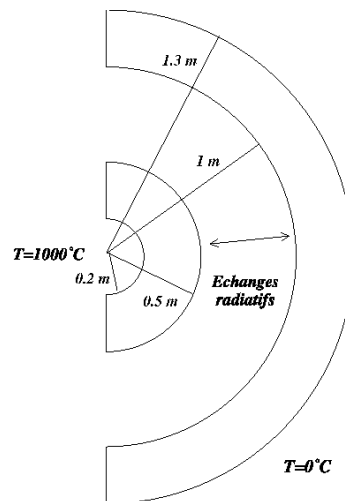


Figure 14.1: Solid domain

#### 14.1.2 Physical conditions

The solid is related to steel having following physical characteristics :

- conductivity  $k = 25 \text{ W/mK}$
- density  $\rho = 7700 \text{ kg/m}^3$
- specific heat  $C_p = 460 \text{ J/kgK}$

### 14.1.3 Initial conditions, boundary conditions

Initially (at  $t = 0$ ), the solid is at  $0^\circ C$ . We impose on the inner surface of the inner sphere a temperature  $T_1 = 1000^\circ C$  and on the outer surface of the outer sphere a temperature  $T_4 = 0^\circ C$ .

## 14.2 Analytical solution

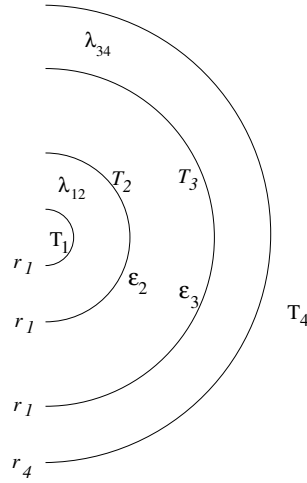


Figure 14.2: 2 concentric spheres

In the case of 2 concentric spheres, the flux  $\varphi$  that passes through the surfaces is solution of the equation

$$\varphi \left( \frac{1}{\epsilon_2} + \frac{s_2}{s_3} \left( \frac{1}{\epsilon_3} - 1 \right) \right) - s_2 \sigma \left[ \left( T_1 + \frac{\varphi r_2^2}{s_2 \lambda_{12}} \left( \frac{1}{r_1} - \frac{1}{r_2} \right) \right)^4 - \left( T_4 - \frac{\varphi r_3^2}{s_3 \lambda_{34}} \left( \frac{1}{r_3} - \frac{1}{r_4} \right) \right)^4 \right] = 0$$

In the present case we have following data :

- conductivities  $\lambda_{12} = \lambda_{34} = 25 \text{ W/mK}$
- emissivities  $\epsilon_2 = 0.5, \epsilon_3 = 0.8$
- edge temperatures  $T_1 = 1000^\circ C, T_4 = 0^\circ C$
- radii  $r_1 = 0.2, r_2 = 0.5, r_3 = 1., r_4 = 1.3$
- surfaces  $s_2 = 4\pi r_2^2, s_3 = 4\pi r_3^2$

Solution of previous equation is then  $\varphi = 44316.66273 \text{ W/m}^2$ . Then we obtain inner walls temperatures

$$T_2 = T_1 - \frac{\varphi r_2^2 \left( \frac{1}{r_1} - \frac{1}{r_2} \right)}{(s_2 \lambda_{12})} = 576.8070439^\circ C$$

$$T_3 = T_4 + \frac{\varphi r_3^2 \left( \frac{1}{r_3} - \frac{1}{r_4} \right)}{(s_3 \lambda_{34})} = 32.5533043^\circ C$$

Temperature profile in a radius of the inner sphere is given by

$$T(r) = \frac{T_1 - T_2}{r \left( \frac{1}{T_1} - \frac{1}{T_2} \right)} + T_1 - \frac{T_1 - T_2}{1 - \frac{r_1}{r_2}}$$

and temperature profile in a radius of the outer sphere by

$$T(r) = \frac{T_3 - T_4}{r\left(\frac{1}{T_3} - \frac{1}{T_4}\right)} + T_3 - \frac{T_3 - T_4}{1 - \frac{r_3}{r_4}}$$

Like in the previous case (CYLINDRES\_2D\_RAY), density and heat capacity disappear at steady state.

## 14.3 Calculation description

### 14.3.1 Meshes

The mesh is realised in 2D, it uses axisymmetry property of the problem, this leads to mesh only a slice of spheres.

The mesh counts :

- 1 482 nodes
- 672 triangles

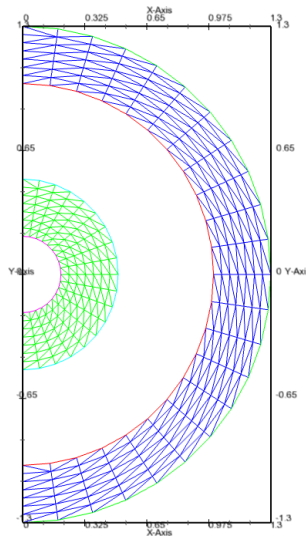


Figure 14.3: Conduction meshes

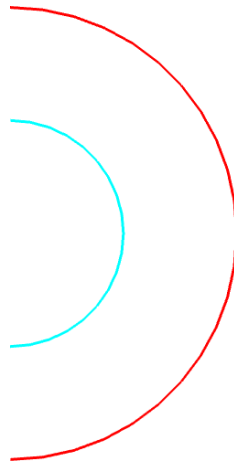


Figure 14.4: Mesh for radiation

Regarding radiation, the mesh is formed by 2 circular arcs of respective radii 0.5 m and 1 m. It counts of 56 faces.

## 14.4 Presentation of results

We have performed calculation with a time step equal to 200 seconds. Convergence has been reached after about 100 000 physical seconds (about 28 hours), with 500 time steps.

### 14.4.1 Temperature field inside the spheres

Figure 14.5 presents the temperature at convergence.

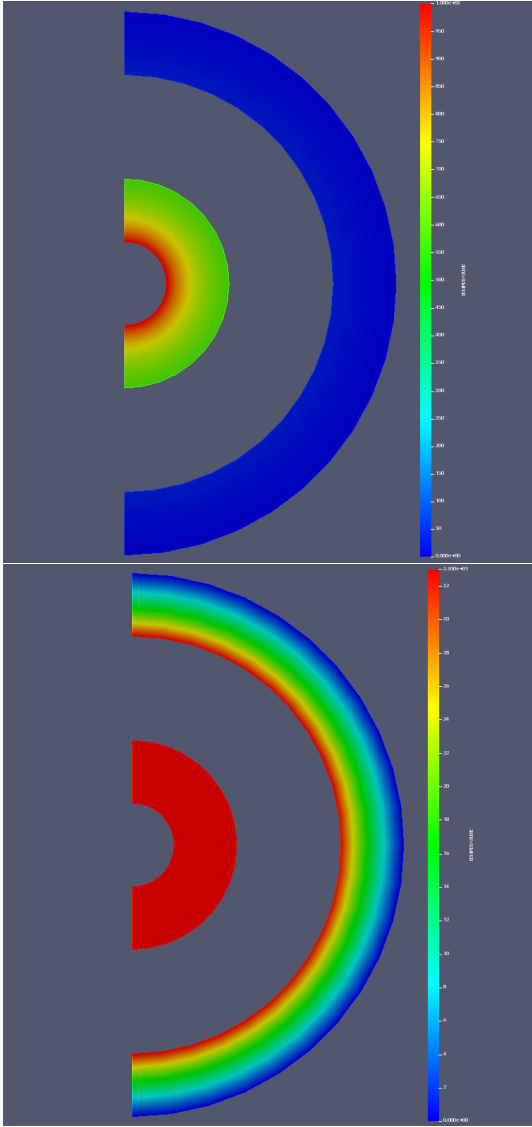


Figure 14.5: Temperature profile at convergence

The figure 14.6 presents temperature domain field at convergence but with a scale which allows to visualize warming of the outer sphere. We also present the temperature profile at  $y=0$ .

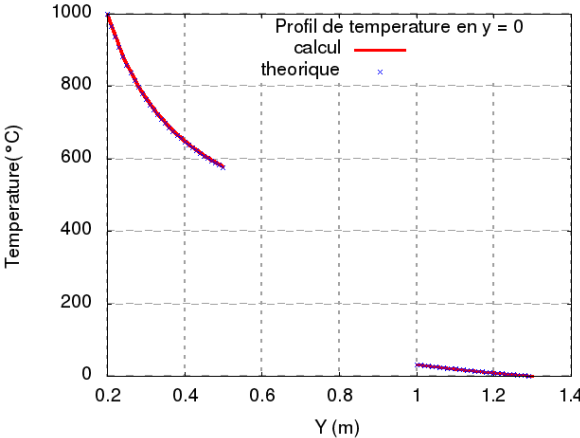


Figure 14.6: Temperature field at convergence

### 14.4.2 Comparison calculation results / analytical values

Comparisons between calculated values of temperature and analytical values are plotted along a radius of the spheres.

We can compare temperature values in  $r = 0.5$  and  $r = 1$

Ordonate	analytical T	T SYRTHES
0.5	5.768070439e+02	5.782931957e+02
1.	3.25533043e+01	3.226574813e+01

Remarks :

- *There is an error here slightly more important. It is possible that it is due to the spatial discretization error of the sphere which is approached by faces.*

#### Comparisons between analytical and calculated profiles

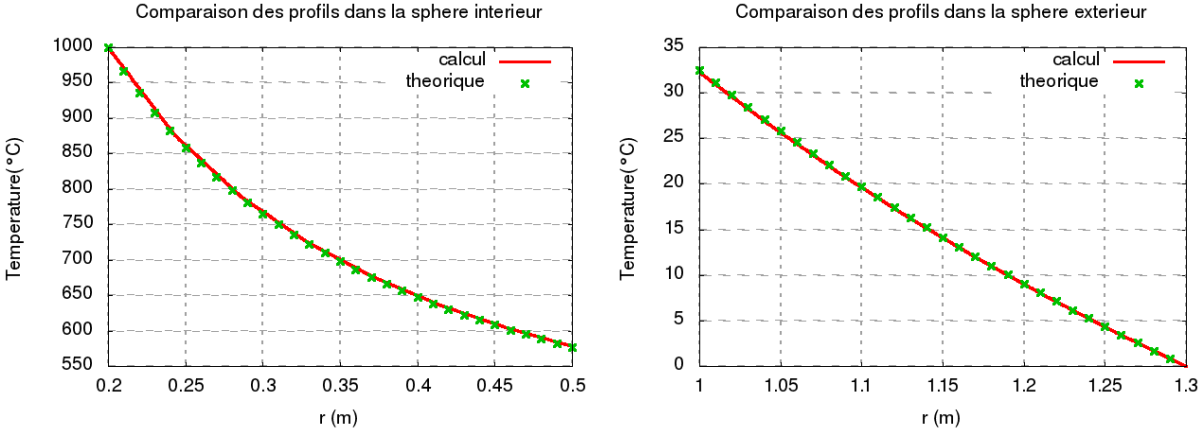


Figure 14.7: Inner sphere

Outer sphere

### 14.4.3 Study of calculation's convergence

The following figure shows temperature's evolution in 6 points along  $y=0$  :  $x=0.3$  (A),  $x=0.4$  (B),  $x=0.5$  (C),  $x=1$ . (D),  $x=1.1$  (E),  $x=1.2$  (F).

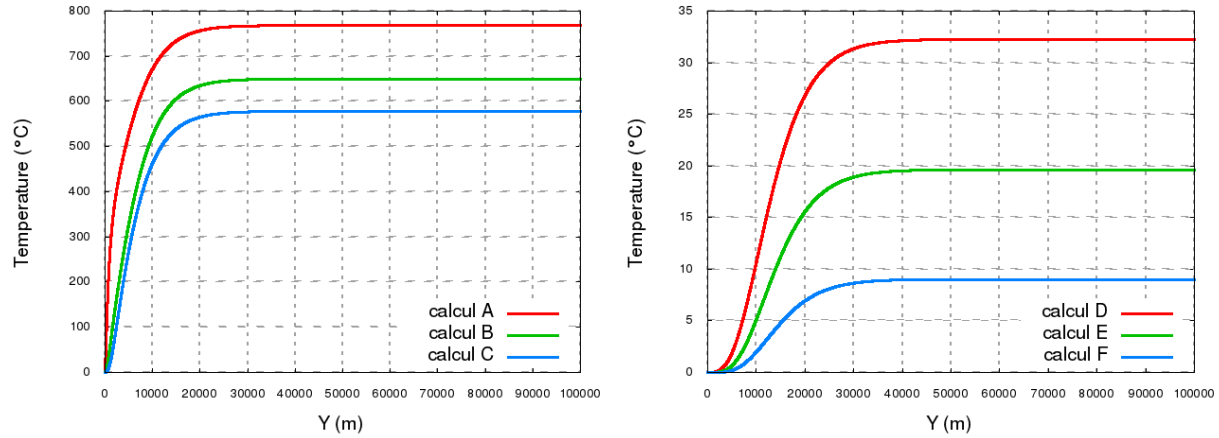


Figure 14.8: Inner sphere

Outer sphere

## 14.5 Synthesis

Results obtained with SYRTHES on this case are satisfactory.

This configuration has allowed to check particularly several aspects :

- calculation of view factors in 2D axisymmetric,
- calculation of shadowing in 2D axisymmetric,
- calculation of elementary matrices in 2D axisymmetric,
- coupling in conduction and radiation in 2D axisymmetric.

## Chapter 15

# CYLINDERS\_3D\_RAY

**Characteristics :** 3D, steady state, cartesian periodicity, conduction/radiation coupling.

**Objectives :** Validation of radiative calculation in 3D cartesian with shadowing calculation and taking into account of periodicity of rotation. Validation of conduction/radiation coupling.

### 15.1 Test case description

#### 15.1.1 Geometry

Consider two concentric cylinders. Cylinders are assumed of infinite length and are modeled in 3D. For calculation, we chose a sufficient length in order to minimize influence of radiative boundary condition which is necessary to give at the ends of the domain.

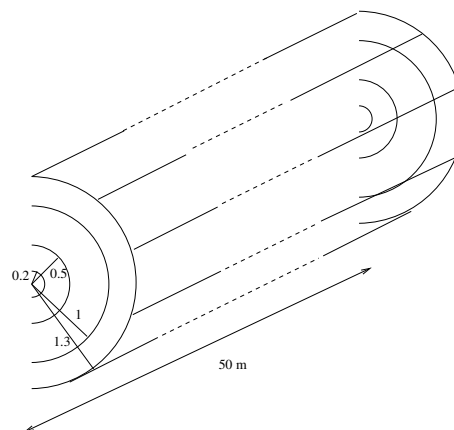


Figure 15.1: Solide domain

#### 15.1.2 Physical conditions

The solid is related to steel having following physical characteristics :

- conductivity  $k = 25 \text{ W/mK}$
- density  $\rho = 7700 \text{ kg/m}^3$
- specific heat  $C_p = 460 \text{ J/kgK}$

### 15.1.3 Initial conditions, boundary conditions

Initially (at  $t = 0$ ), the solid is at  $0^\circ C$ . We impose on the inner surface of the inner cylinder a temperature  $T_1 = 1000^\circ C$  and on the outer surface of the outer cylinder a temperature  $T_4 = 0^\circ C$ .

## 15.2 Analytical solution

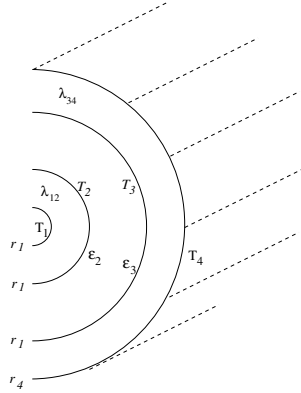


Figure 15.2: 2 infinite concentric cylinder

In the case of 2 concentric cylinder, the flux  $\varphi$  which passes through the surfaces is a solution of the equation

$$\varphi \left( \frac{1}{\varepsilon_2} + \frac{r_2}{r_3} \left( \frac{1}{\varepsilon_3} - 1 \right) \right) - s_2 \sigma \left[ \left( T_1 + \frac{\varphi r_1 \log \frac{r_1}{r_2}}{s_1 \lambda_{12}} \right)^4 - \left( T_4 - \frac{\varphi r_4 \log \frac{r_3}{r_4}}{s_4 \lambda_{34}} \right)^4 \right] = 0$$

In present case we have following data :

- conductivities  $\lambda_{12} = \lambda_{34} = 25 \text{ W/mK}$
- emissivities  $\varepsilon_2 = 0.5, \varepsilon_3 = 0.8$
- edge temperatures  $T_1 = 1000^\circ C, T_4 = 0^\circ C$
- radii  $r_1 = 0.2, r_2 = 0.5, r_3 = 1., r_4 = 1.3$
- surfaces  $s_1 = 2\pi r_1, s_2 = 2\pi r_2, s_3 = 2\pi r_3, s_4 = 2\pi r_4$

Solution of previous equation is then  $\varphi = 59706.82602 \text{ W/m}^2$

Then we obtain inner walls temperatures

$$T_2 = T_1 + \varphi \frac{\log \frac{r_1}{r_2}}{2\pi \lambda_{12}} = 651.712890^\circ C$$

$$T_3 = T_4 - \varphi \frac{\log \frac{r_3}{r_4}}{2\pi \lambda_{34}} = 99.7260894^\circ C$$

Temperature profile in a radius of the inner cylinder is given by

$$T(r) = T_1 + \frac{T_1 - T_2}{\log \frac{r_1}{r_2}} \log \frac{r}{r_1}$$

and temperature profile in a radius of the outer cylinder by

$$T(r) = T_4 + \frac{T_3 - T_4}{\log \frac{r_3}{r_4}} \log \frac{r}{r_4}$$

## 15.3 Calculation description

### 15.3.1 Meshes

The mesh is realised in 3D. We have meshed 1/8 of cylinders. Conditions of periodicity are used during calculation.

The mesh has :

- 51 408 nodes,
- 33630 tetrahedra.

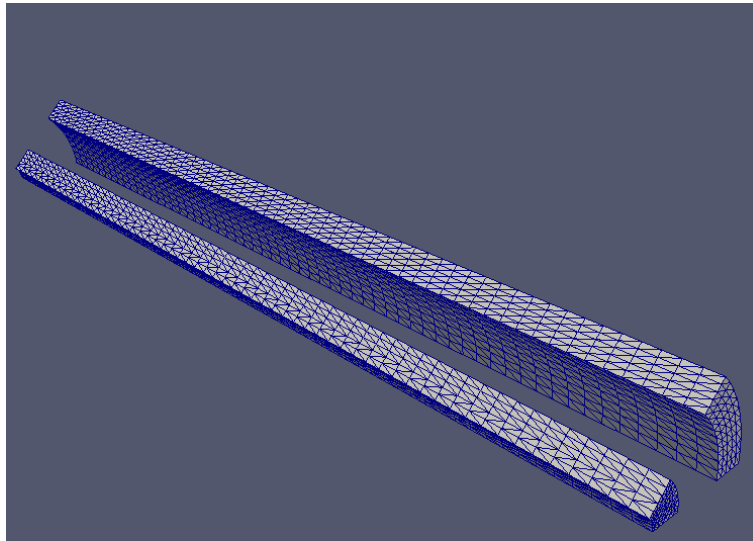


Figure 15.3: Mesh for conduction

Regarding radiation, the mesh consist of 2012 facets. In order to close the domain, we impose at both ends a null flux condition (in order to minimize influence of extremities).

Remarks :

*In this 3D case, space discretization is coarser than in the 2D case seen in previous paragraph. Indeed, the radiation mesh has already 2012 facets for 1/8 domain this will lead to view factor calculation for some 16096 facets even if, ultimately, only 2 025 078 view factors will be stored (instead of calculation and storage of the 129 548 656 view factors if the whole domain had been meshed !)*

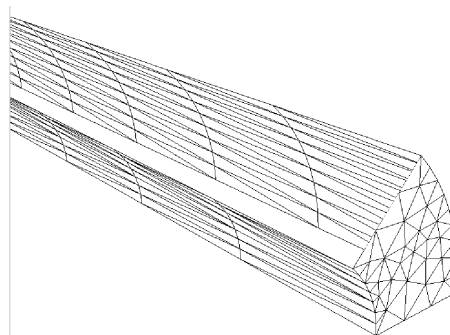


Figure 15.4: Radiation mesh

## 15.4 Presentation of results

We have performed calculation with a time step equal to 200 seconds. Convergence has been reached after about 100 000 physical seconds (about 28 hours), with 500 time steps.

### 15.4.1 Temperature inside cylinders

We present here the temperature field at convergence.

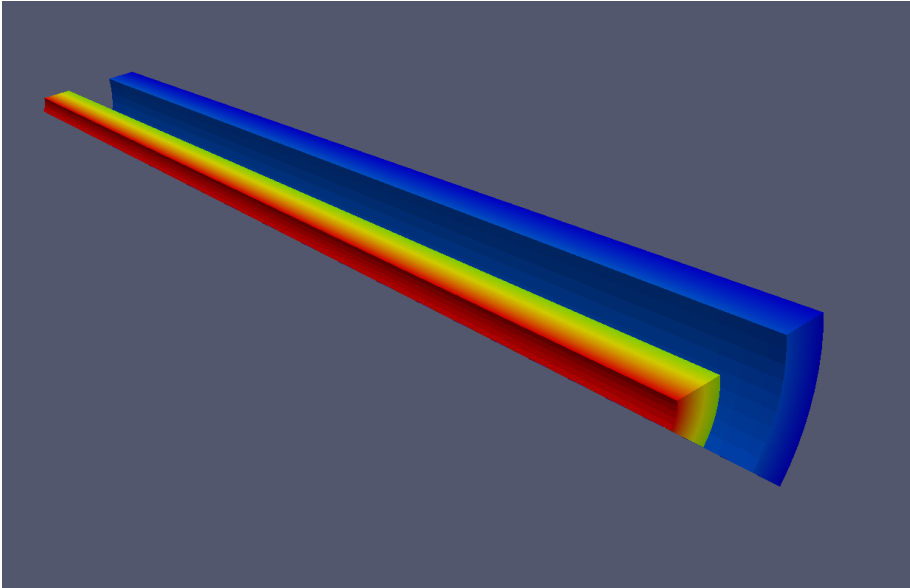


Figure 15.5: Temperature domain at convergence

The figure 15.6 present temperature domain at convergence but with different scales which allow to visualize isotherms inside inner and outer cylinders.

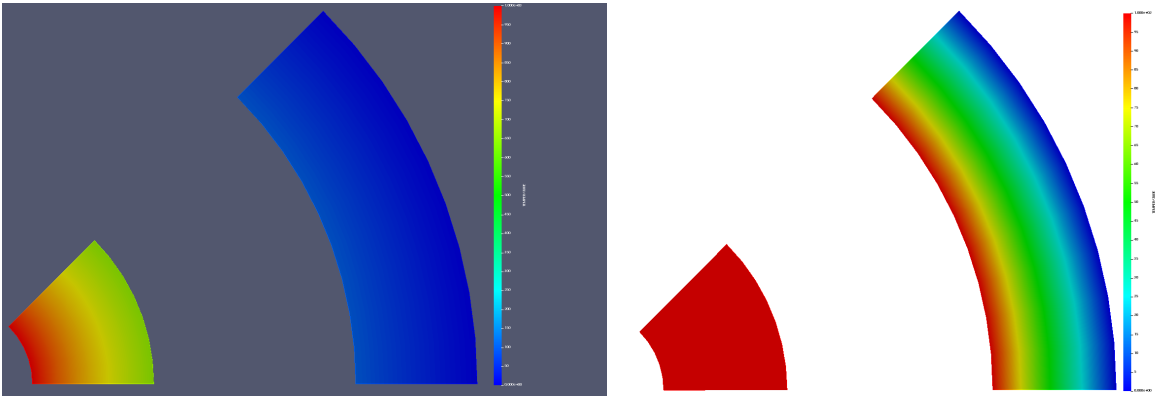


Figure 15.6: Temperature at convergence



## 15.5 Synthesis

Results obtained with SYRTHES on this case are satisfactory.

It should be noted that this configuration is much more heavier to use because it's necessary a domain of great length in order to minimize effect of boundary conditions to the ends. We have then numbers of nodes and facets relatively large.

This configuration has allowed to check several aspects particularly :

- conduction mesh reading (volumetric) and radiation (surface) in 3D,
- calculation of view factor in 3D,
- calculation of shadowing in 3D,
- taking into account of periodicity. Note the good result, related to the fact that periodicity is treated rigorously. In this particular case, the benefit of time and of memory space is significant : we compute and store  $8 \times 2012 \times 2013 / 2 = 16\,200\,624$  quad integrals instead of  $16096 \times 16097 / 2 = 129\,548\,656$  if integrality of the domain had been meshed.
- consideration of coupling and null flux boundary conditions (on the ends),
- calculation of elementary conduction matrices in 3D,
- numerical coupling in conduction and radiation.

It should be noted that similar remarks to those made in the test case "RING" concerning faceting of the structure can be made. Add to this the fact that analytical solution implies an infinitely long domain along cylinders's axis. Here infinite length introduce an "inaccuracy" in the distribution of energy (even if it remains modest because of the length modeled).

Part III

HEAT AND MASS TRANSFERS

# Chapter 16

## WOODPANEL

**Characteristics :** Wall with constant boundary conditions (temperature and vapor pressure).

**Objectives :** We wish to estimate the profile of temperature and humidity in a timber insulation board of medium density insulation board. It is located in a theoretical situation, where the boundary conditions are constant for each side wall (outer atmosphere, and internal conditions), and wherein the upper and lower faces are isolated (heat and moisture).

### 16.1 Test case description

#### 16.1.1 Geometry

The wall is made exclusively of a wood fiber material of medium density, with a height of 1 meter. The outer faces are flat and parallel. The wall thickness of 8 cm.

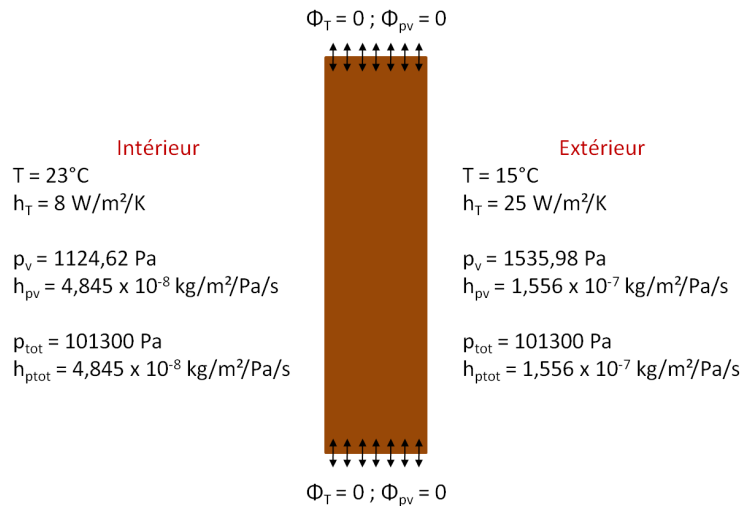


Figure 16.1: Solid domain

#### 16.1.2 Physical conditions

In all material, the initial conditions are :

- $T = 23^\circ\text{C}$
- $p_v = 1124,62\text{Pa}$

### 16.1.3 Boundary conditions

The boundary conditions are given in the table below :

Ambiance	$T(^{\circ}C)$	$h_T (W/m^2/K)$	$p_v (Pa)$	$h_{pv} (kg/m^2/s/Pa)$	$p_t (Pa)$	$h_{pt} (kg/m^2/s/Pa)$
Indoor	23	8	1124.6	$4.845 \cdot 10^{-8}$	101300	$4.845 \cdot 10^{-8}$
Outdoor	15	25.1	1535.98	$1.556 \cdot 10^{-7}$	101300	$1.556 \cdot 10^{-7}$

## 16.2 Calculation description

### 16.2.1 Meshes

The mesh is realized in 2 dimensions. It counts :

- 6 320 nodes,
- 12 324 triangles.

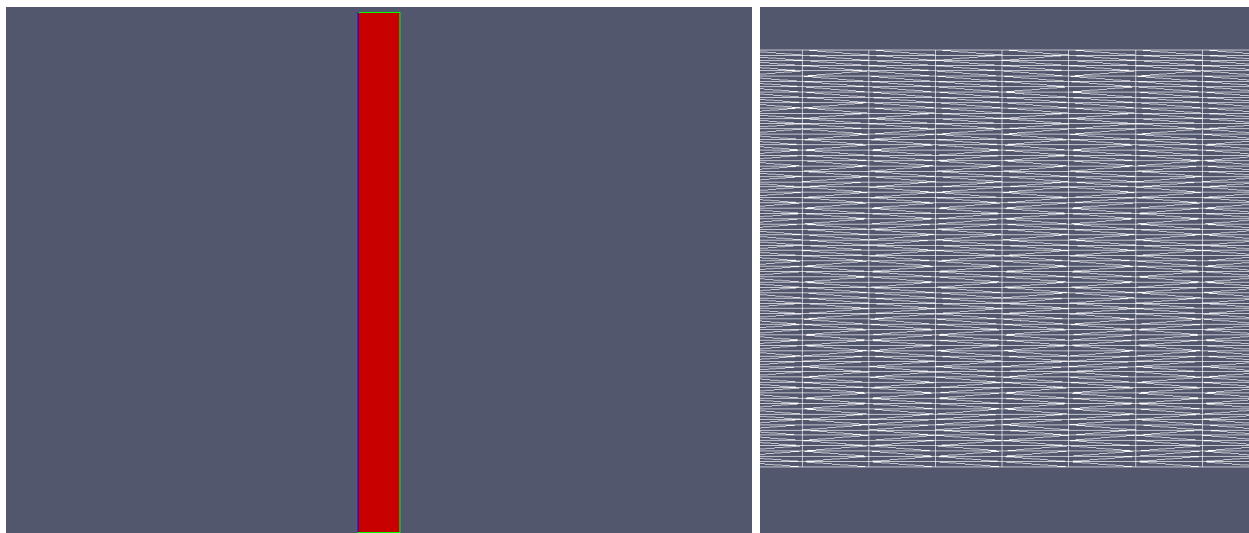


Figure 16.2: Solid mesh and zoom

The mesh references are given in the table below :

Description	Type	Reference
A timber insulation board MDF	Volume (material)	1
Ambiance outdoor	Surface (boundary condition)	1
Ambiance indoor	Surface (boundary condition)	2
Flux null, on the upper and lower faces of the panel	Surface (boundary condition)	0

## 16.3 Presentation of results

We have performed calculation with a time step equal to 60 seconds. Convergence has been reached after about 6105 physical seconds (about 6,95 days), with 10000 time steps. we consider the following results, reports every hour:

- Changes in temperature and humidity depending on the thickness of the panel (all cm)
- Field temperatures at the end of the simulation

- Field vapor pressures, HR and volumetric water rates at the end of the simulation
- Mass balances in the volume

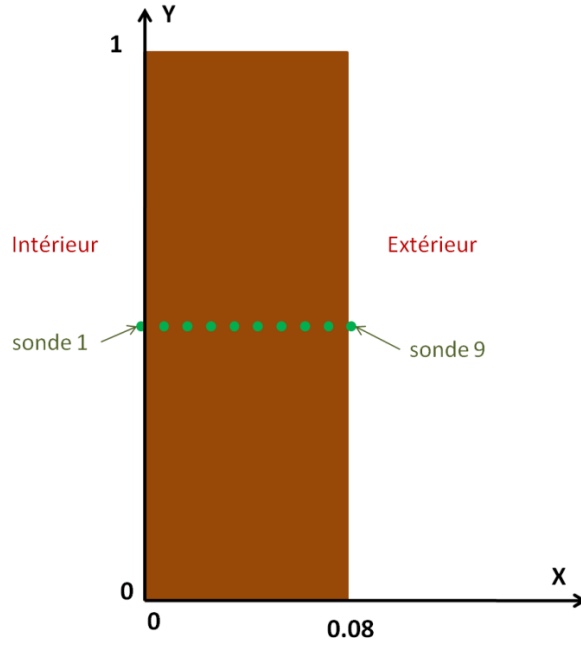


Figure 16.3: Probes

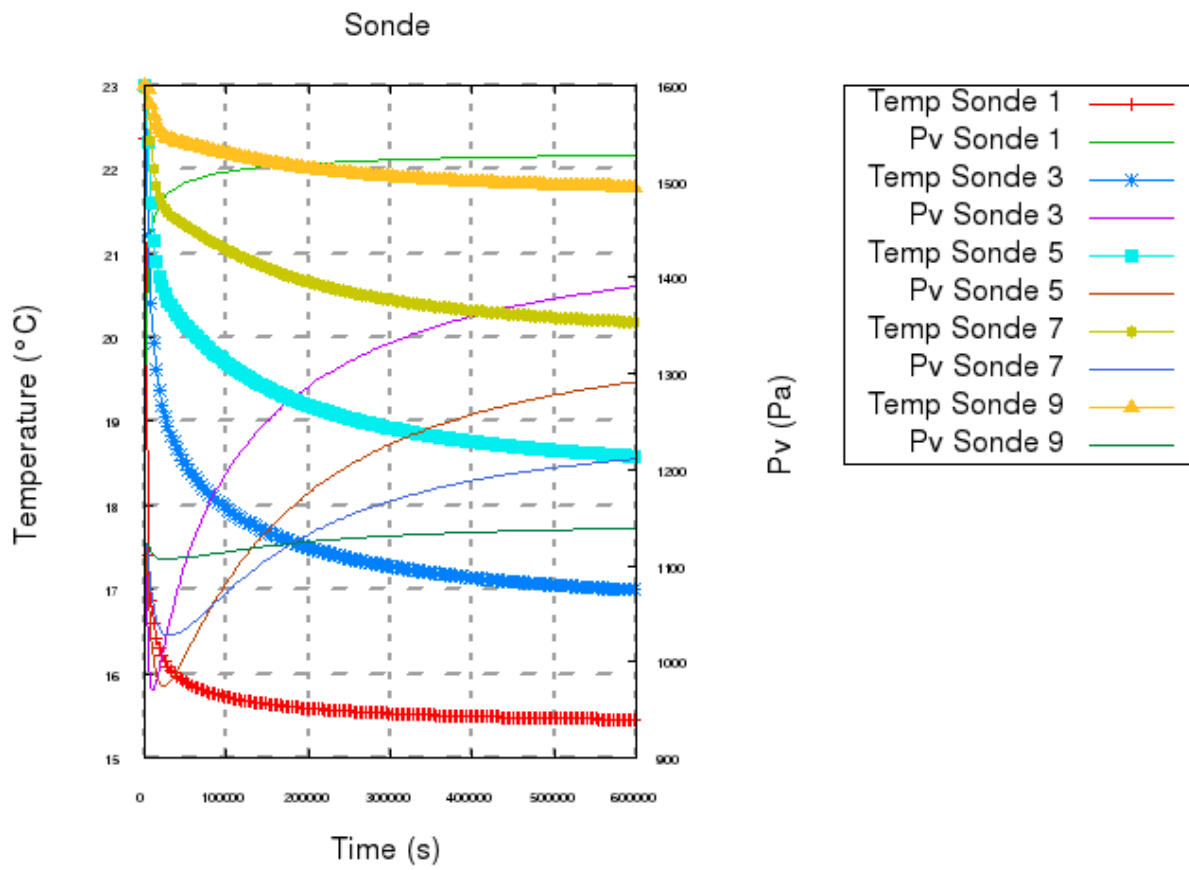


Figure 16.4: Probes

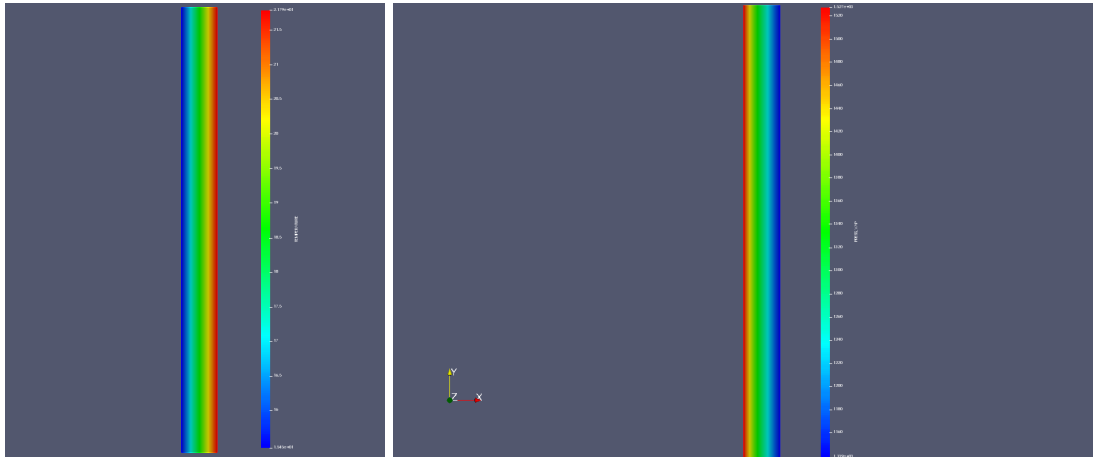


Figure 16.5: Temperature (on the left) and vapour pressure (on the right) at convergence

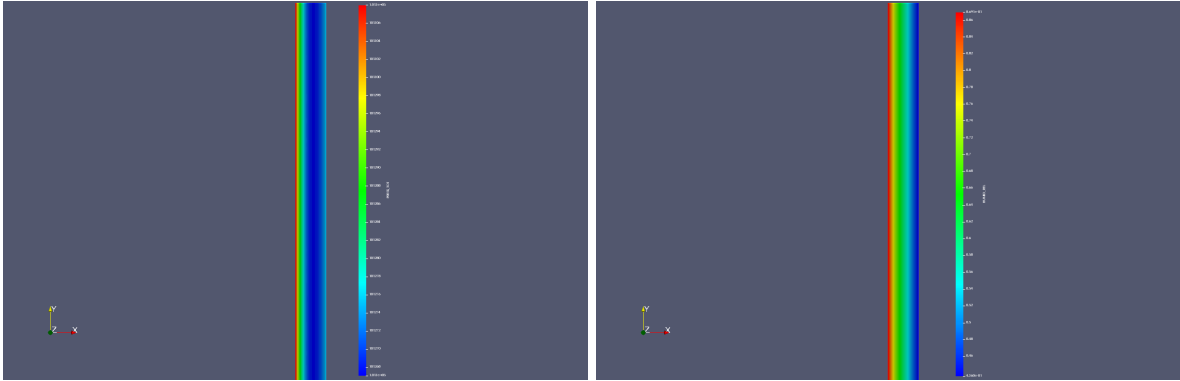


Figure 16.6: Total pressure (on the left) and relative humidity (on the right) at convergence

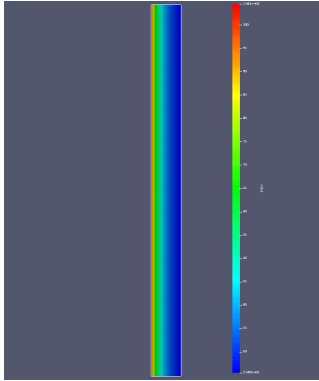


Figure 16.7: Volumic moisture level at convergence

# Bibliography

- [1] Péniguel C. Heat transfer simulation for industrial applications : Needs, limitations, expectations. pages 102–114. Int Journal of Heat and Fluid Flow (vol 19), Elsevier, 1998.
- [2] Rupp I , Péniguel C. Coupling heat conduction and radiation and convection phenomena in complex 2D and 3D geometries. U.K. Swansea, 1997. Numerical Methods in Thermal Problems.
- [3] Rupp I , Péniguel C. Coupling heat conduction, radiation and convection in complex geometries. Int Journal of Numerical Methods for Heat and Fluid Flow - Vol 9, 1999.
- [4] Rupp I, Péniguel C. *SYRTHES - Conduction et rayonnement thermique - Manuel théorique de la version 3.1*. Rapport EDF/DER HE-41/98/048A.
- [5] Sparrow E M, CESS R D. *Radiation Heat Transfer*.
- [6] Péniguel C , Rupp I. Coupling conduction radiation and convection using PVM. St Venant Symp. Paris, 1997.
- [7] Péniguel C, Rupp I. A numerical method for thermally coupled fluid and solid problems. pages 1027–1039, U.K. Swansea, 1993. Numerical Methods in Thermal Problems.
- [8] Péniguel C, Rupp I. A finite element approach to simulate general conduction problems. pages 555–562, U.K. Southampton, 1994. 3rd Int Conference Heat Transfer.
- [9] Péniguel C, Rupp I. A numerical approach for thermally coupled fluid and solid problems in complex geometries. pages 27–34, U.K. Southampton, 1994. 3rd Int Conference Heat Transfer.
- [10] Péniguel C, Rupp I. A numerical approach of coupled heat conduction and enclosure radiation problems. pages 787–796, Italy - Venezia, 1995. 8th FEMIF.
- [11] Péniguel C, Rupp I. A numerical approach of thermal problems coupling fluid solid and radiation in complex geometries. pages 797–806, Italy - Venezia, 1995. 8th FEMIF.
- [12] Péniguel C, Rupp I. Coupling heat conduction and radiation in complex 2D and 3D geometries. U.K. Swansea, 1997. Numerical Methods in Thermal Problems.
- [13] Carslow HS, Jaeger JC. *Conduction of Heat in Solids*. Second edition, Oxford University Press, 1959.
- [14] Siegel R, Howell JR. *Thermal Radiation Problem*. Second edition, Hemisphere Publishing Corporation, New York.